

The $\gamma\gamma \rightarrow \phi_i\phi_j$ processes in the type-III two-Higgs-doublet model

J. Hernández-Sánchez*

*Fac. de Cs. de la Electrónica, Benemérita Universidad Autónoma de Puebla,
Apdo. Postal 542, 72570 Puebla, Puebla, México,
and Dual C-P Institute of High Energy Physics, México.*

C. G. Honorato and M. A. Pérez

Departamento de Física, CINVESTAV, Apartado Postal 14-740, 07000 México, D. F., México.

J. J. Toscano†

*Facultad de Ciencias Físico Matemáticas, Benemérita Universidad
Autónoma de Puebla, Apartado Postal 1152, Puebla, Puebla, México.*

(Dated: November 21, 2018)

We discuss the implications of assuming a four-zero Yukawa texture and a general Higgs potential for the production of neutral Higgs boson pairs at $\gamma\gamma$ colliders through the $\gamma\gamma \rightarrow \phi_i\phi_j$ ($\phi_i = h, H, A$) reaction within the context of the two Higgs doublet model type III. Exact analytical expressions for the $\gamma\gamma \rightarrow \phi_i\phi_j$ reaction are presented. The use of a nonlinear R_ξ -gauge, which considerably simplifies the loop calculations and renders compact analytical expressions, is stressed. We show that these processes are very sensitive to a general structure of the Higgs potential that impact the triple and quartic couplings of the scalar sector. We present results for scenarios of the parameters of the model that are still consistent with current experimental constraints. It is found that the cross sections for the $\gamma\gamma \rightarrow \phi_i\phi_j$ processes can be up to two orders of magnitude larger than those gotten in 2HDM type I and type II. The possibility of a light CP-scalar is also studied.

PACS numbers: 12.60.Fr, 14.80.Cp

I. INTRODUCTION

The discovery of a Higgs boson (or several Higgs bosons) is central to the broad experimental programs of both the Large Hadron Collider (LHC) and the International Linear Collider (ILC) [1], either through e^-e^+ collisions or via the secondary $\gamma\gamma$ and γe modes [2, 3]. If there is a Higgs boson, it is almost certain to be found at the LHC and its mass measured by the ATLAS [4] and CMS [5] experiments. Then, in the much cleaner environment of the ILC a more complete and precise experimental analysis can be carried out to verify if it corresponds to a Standard Model (SM) Higgs or other type of scalar particle. The high level of complementarity between both type of colliders has broadly been studied by diverse groups [6]. Whereas LHC has a large mass reach for direct discoveries due its high collision energy, the ILC enables precise measurements and therefore detailed studies of direct productions of new particles as well as high sensitivity to indirect effects of heavier new particles. It has been found that some processes occurring via γe or $\gamma\gamma$ collisions are complementary to their analogous reactions at e^+e^- collisions as the former are more appropriate to study the bosonic sector of the SM. In particular, $\gamma\gamma$ collisions have been recognized as an invaluable tool to probe the structure of electroweak interactions at high energies, both in the gauge and the Higgs sectors [7]. In the gauge sector, the reaction $\gamma\gamma \rightarrow WW$ has been widely studied, mainly for testing any physics beyond the SM [8, 9]. As for the Higgs sector, once a Higgs boson is discovered, the one-loop process $\gamma\gamma \rightarrow H \rightarrow X$ might play an important role in determining some properties of this elusive particle, such as mass, total width, CP properties, and couplings to other light particles in a model-independent fashion [10]. Recently, a series of papers have been published in photon-photon collisions on the more traditional types I and II of 2HDM, which spelt out the genuine phenomenological features that differentiate them from the MSSM [11]. In addition, neutral particle pair production at a $\gamma\gamma$ collider can be highly sensitive to new physics effects as processes of this kind are naturally suppressed because they first arise at the one-loop level, thereby providing a detailed test for the structure of extended Higgs sectors.

It is expected that the LHC will allow us to test the mechanism of Electro-Weak Symmetry Breaking (EWSB), which represents a unique probe of a weakly-interacting theory, as is the case of the Minimal Supersymmetric Standard Model

*Electronic address: jaimeh@ece.buap.mx

†Electronic address: jtoscana@cfm.buap.mx

(MSSM) [12] and general 2HDMs of Type I, II, X and Y (2HDM-I, 2HDM-II, 2HDM-X and 2HDM-Y) [13, 14, 15]¹, or whether strongly-interacting scenarios are instead realized, like in the old Technicolor models or the ones discussed more recently [19].

The 2HDM-II has been quite attractive to date, in part because it coincides with the Higgs sector of the MSSM, wherein each Higgs doublet couples to the u - or d -type fermions separately. However, this is only valid at tree-level [20, 21]. When radiative effects are included, it turns out that the MSSM Higgs sector corresponds to the most general version of the 2HDM, namely the 2HDM-III, whereby both Higgs fields couple to both quarks and leptons. Thus, we can consider the 2HDM-III as a generic description of physics at a higher scale (of order TeV or maybe even higher), whose low energy imprints are reflected in the Yukawa coupling structure. The general 2HDM has a potential problem with flavor changing neutral currents (FCNC) mediated by the Higgs boson, which arise when each type of quark (u and d) is allowed to couple to both Higgs doublets, and FCNC could be induced at large rates that may jeopardize the model. The possible solution to this problem of the 2HDM involves an assumption about the Yukawa structure of the model. Then, in order to keep the FCNC problem under control, we can choose one of the following mechanisms: (1) *Discrete symmetries*. This choice is based on the Glashow–Weinberg’s theorem concerning FCNC’s in models with several Higgs doublets [22]. (2) *Radiative suppression*. When a given set of Yukawa matrices are present at tree-level, but the other ones arise only as a radiative effect. This occurs for instance in the MSSM, where the type-II 2HDM structure is not protected by some symmetry, and it is transformed into a type-III 2HDM through loops-effects of sfermions and gauginos [23, 24, 25]. (3) *Flavor symmetries*. Suppression of FCNC effects can also be achieved when a certain form of the Yukawa matrices that reproduce the observed fermion masses and mixing angles is implemented in the model, which is then named as THDM-III. This could be done either by implementing the Frogart-Nielsen mechanism to generate the fermion mass hierarchies [26], or by studying a certain ansatz for the fermion mass matrices [27]. It should be noted, that when this scheme is implemented, the scalar Higgs potential must be expressed in its general form because it is not necessary to impose a discrete symmetry.

In this paper, we will work in the context of the mechanism (3) by implementing the so-called four-texture ansatz for Yukawa matrices. This ansatz, is illustrated in Refs. [28, 29, 30], in which a detailed study of the 2HDM-III Yukawa Lagrangian was presented under the assumption of a specific texture pattern [31], which generalizes the original model of Ref. [32]. Phenomenological implications of the neutral Higgs sector of the model, including Lepton Flavour Violation (LFV) and/or Flavour Changing Neutral Currents (FCNCs) effects, have been studied previously [25, 33]. The extension of such an approach to investigate the charged Higgs boson phenomenology was carried out in Refs. [30, 34], in which the implications of this Yukawa texture for the charged Higgs boson properties (masses and couplings), as well as the resulting pattern of charged Higgs boson decays and main production mechanisms at the LHC are discussed. Here, we will focus on Higgs boson pair production at $\gamma\gamma$ colliders through the $\gamma\gamma \rightarrow \phi_i \phi_j$ reaction,² within the context of this more general version of the two-Higgs doublet model (2HDM-III). We will study the three distinct modes for Higgs boson pair production that are allowed: $\gamma\gamma \rightarrow AA$, $\gamma\gamma \rightarrow A\phi_a$, and $\gamma\gamma \rightarrow \phi_a \phi_b$, with $\phi_a = h, H$. The impact of the Higgs potential on the production of pairs of light Higgs bosons, through the $\gamma\gamma \rightarrow hh$ reaction, has been studied recently [35, 36, 37]. The work of Ref.[35] is focused to study the particular scenario where h couples to gauge bosons and fermions as the SM Higgs particle does, and finds that the cross section for the $\gamma\gamma \rightarrow hh$ process can be much larger than the SM prediction. The same scenario was analyzed in Ref. [36], where it is taken into account the one-loop correction to the hhh vertex. It was found that this effect, together with the one-loop charged Higgs boson contribution, produces a considerable enhancement of the cross section. On the other hand, resonant effects due to the charged Higgs boson and the heavy neutral one H on the $\gamma\gamma \rightarrow hh$ and $\gamma\gamma \rightarrow AA$ processes were studied in [37]. In this paper, we discuss the implications of assuming a four-zero Yukawa texture and general Higgs potential in the framework of the 2HDM-III on all the possible processes $\gamma\gamma \rightarrow \phi_i \phi_j$, which include some scenarios of experimental interest did not considered in Refs. [35, 36, 37]. Apart from presenting analytical expressions for the three distinct reactions, namely $\gamma\gamma \rightarrow \phi_a \phi_b, \phi_a A, AA$, we will analyze their unpolarized cross-sections in some scenarios that are still consistent with the most recent bounds on the model parameters as obtained from electroweak precision measurements [38]. Higgs boson pair production at $\gamma\gamma$ colliders has already been studied in the SM by means of a nonlinear R_ξ -gauge [39], and in the MSSM via a linear R_ξ gauge [40]. Partial results were also obtained within the context of the 2HDM-II [41].

On the other hand, the calculation of $\gamma\gamma \rightarrow \phi_i \phi_j$ scattering is far from trivial, mainly due to the plethora of Feynman

¹ The type-X (type-Y) 2HDM is referred as the type-IV (type-III) 2HDM in Ref. [13] and as the type-I’ (type-II’) 2HDM in Ref. [14, 16]. Sometimes the most general 2HDM, in which each fermion couples to both Higgs doublet fields, is called the type III 2HDM[17]. All variants of the 2HDM were discussed recently in [18]. The version that will be considered in this work will be called simply the 2HDM-III model.

² Throughout the paper, the symbol ϕ_i will stand for any of the three neutral Higgs bosons of the 2HDM, h, H, A , whereas ϕ_a will denote exclusively a CP-even Higgs boson.

diagrams arising in the gauge sector. Such a hard task can be significantly relieved if one uses an appropriate gauge-fixing procedure for the W boson. Rather than using the conventional linear gauge-fixing procedure [42], we will use a nonlinear scheme that is covariant under the electromagnetic group $U_e(1)$ [43]. We will use a general renormalizable nonlinear gauge-fixing procedure for the 2HDM [44], which is intended to remove the most unphysical vertices from the interaction Lagrangian, thereby facilitating the calculation of radiative corrections considerably. It turns out that this class of gauges is tailored for the calculation of $\gamma\gamma \rightarrow \phi_i\phi_j$ scattering. We will show that such a gauge not only reduces dramatically the number of Feynman diagrams, but renders manifestly gauge-invariant and ultraviolet-finite amplitudes. The relevance of nonlinear R_ξ gauges [43] to the calculation of radiative corrections has been emphasized by several authors not only within the context of the SM [39, 45, 46], but in some of its extensions such as the 2HDM [47], the so-called 331 model [48], and also in the model independent effective Lagrangian approach [49].

The paper is organized as follows. In Sec. II the main features of the Higgs-Yukawa sector of the 2HDM-III model are discussed. In Sec. III, the main ingredients of the nonlinear R_ξ -gauge appropriate for this model are presented. Sec. IV is devoted to the cross-sections for $\gamma\gamma \rightarrow \phi_i\phi_j$ scattering, whereas numerical results are analyzed in Sec. V. Finally, the conclusions are presented in Sec. VI.

II. THE HIGGS-YUKAWA SECTOR OF THE GENERAL TWO HIGGS DOUBLET MODEL

In this section, we will discuss the main features of the general Higgs potential and the implementation of a specific four-zero texture in the Yukawa matrices within the 2HDM-III. When a flavor symmetry in the Yukawa sector is implemented, discrete symmetries in the Higgs potential are not needed, so the most general Higgs potential must be introduced.

A. The general Higgs potential in the 2HDM-III

The 2HDM incorporates two scalar doublets of hypercharge +1: $\Phi_1^\dagger = (\phi_1^-, \phi_1^{0*})$ and $\Phi_2^\dagger = (\phi_2^-, \phi_2^{0*})$. The most general gauge invariant and CP-conserving potential can be written as [50]

$$\begin{aligned} V(\Phi_1, \Phi_2) = & \mu_1^2(\Phi_1^\dagger\Phi_1) + \mu_2^2(\Phi_2^\dagger\Phi_2) - \left(\mu_{12}^2(\Phi_1^\dagger\Phi_2) + \text{H.c.} \right) + \frac{1}{2}\lambda_1(\Phi_1^\dagger\Phi_1)^2 + \frac{1}{2}\lambda_2(\Phi_2^\dagger\Phi_2)^2 + \lambda_3(\Phi_1^\dagger\Phi_1)(\Phi_2^\dagger\Phi_2) \\ & + \lambda_4(\Phi_1^\dagger\Phi_2)(\Phi_2^\dagger\Phi_1) + \left(\frac{1}{2}\lambda_5(\Phi_1^\dagger\Phi_2)^2 + \left(\lambda_6(\Phi_1^\dagger\Phi_1) + \lambda_7(\Phi_2^\dagger\Phi_2) \right) (\Phi_1^\dagger\Phi_2) + \text{H.c.} \right), \end{aligned} \quad (1)$$

where all parameters are assumed to be real³. In many discussions of the 2HDM, the terms proportional to λ_6 and λ_7 are absent, as happens in the 2HDM type I and II where the discrete symmetry $\Phi_1 \rightarrow \Phi_1$ and $\Phi_2 \rightarrow -\Phi_2$ is imposed in order to avoid dangerous flavor changing neutral current (FCNC) effects. However, in our model where mass matrices with a four-texture are considered, it is not necessary to implement the above discrete symmetry. Therefore, we must keep the terms proportional to λ_6 and λ_7 . As we will show below, these parameters play an important role in the $\gamma\gamma \rightarrow \phi_i\phi_j$ reactions. It is worth commenting that the parameters λ_6 and λ_7 are essential to obtain the decoupling limit of the model in which only one CP-even scalar is light. As long as these terms exist, there are two independent energy scales, v and Λ_{THDM} , and the spectrum of Higgs boson masses is such that m_h is of the order of v , whereas m_H , m_A and m_{H^\pm} are all of the order of Λ_{THDM} [50]. In this case, all of the heavy Higgs bosons decouple in the limit of $\Lambda_{\text{THDM}} \gg v$, according to the decoupling theorem. On the other hand, when the scalar potential does respect the discrete symmetry, it is impossible to have two independent energy scales [50]. As a consequence, all of the physical scalar masses lie on the Fermi scale v . Since v is already fixed by the experiment, a very heavy Higgs boson can only arise through a large dimensionless coupling constant λ_i . In this scenario the decoupling theorem is no longer valid, thereby opening the possibility for the appearance of nondecoupling effects. In addition, since the scalar potential contains some terms that violate the $SU(2)$ custodial symmetry, nondecoupling effects can arise in one-loop induced Higgs boson couplings [51].

The scalar potential (1) has been diagonalized to yield the mass-eigenstates fields. The charged components of the doublets lead to a physical charged Higgs boson and the pseudo-Goldstone boson associated with the W gauge field:

$$G_W^\pm = \phi_1^\pm c_\beta + \phi_2^\pm s_\beta, \quad (2)$$

$$H^\pm = -\phi_1^\pm s_\beta + \phi_2^\pm c_\beta, \quad (3)$$

³ The λ_6 and λ_7 parameters are complex in general, but we will assume that they are real by simplicity.

with $\tan \beta = v_2/v_1 \equiv t_\beta$, being $v_1/\sqrt{2}$ ($v_2/\sqrt{2}$) the vacuum expectation value (VEV) associated with Φ_1 (Φ_2), and

$$m_{H^\pm}^2 = \frac{\mu_{12}^2}{s_\beta c_\beta} - \frac{1}{2}v^2(\lambda_4 + \lambda_5 + t_\beta^{-1}\lambda_6 + t_\beta\lambda_7), \quad (4)$$

where we have introduced the shorthand notation $s_\beta = \sin \beta$ and $c_\beta = \cos \beta$. On the other hand, the imaginary part of the neutral components ϕ_{iI}^0 defines the neutral CP-odd scalar and the pseudo-Goldstone boson associated with the Z gauge boson. The corresponding rotation is given by

$$G_Z = \phi_{1I}^0 c_\beta + \phi_{2I}^0 s_\beta, \quad (5)$$

$$A = -\phi_{1I}^0 s_\beta + \phi_{2I}^0 c_\beta, \quad (6)$$

where

$$m_A^2 = m_{H^\pm}^2 + \frac{1}{2}v^2(\lambda_4 - \lambda_5). \quad (7)$$

Finally, the real part of the neutral components of the ϕ_{iR}^0 doublets defines the CP-even Higgs bosons h and H . The mass matrix has the form:

$$M_{Re} = \begin{pmatrix} m_{11} & m_{12} \\ m_{12} & m_{22} \end{pmatrix}, \quad (8)$$

where

$$m_{11} = m_A^2 s_\beta^2 + v^2(\lambda_1 c_\beta^2 + s_\beta^2 \lambda_5 + 2s_\beta c_\beta \lambda_6), \quad (9)$$

$$m_{22} = m_A^2 c_\beta^2 + v^2(\lambda_2 s_\beta^2 + c_\beta^2 \lambda_5 + 2s_\beta c_\beta \lambda_7), \quad (10)$$

$$m_{12} = -m_A^2 s_\beta c_\beta + v^2((\lambda_3 + \lambda_4)s_\beta c_\beta + \lambda_6 c_\beta^2 + \lambda_7 s_\beta^2). \quad (11)$$

The physical CP-even states, h and H , are written as

$$H = \phi_{1R}^0 c_\alpha + \phi_{2R}^0 s_\alpha, \quad (12)$$

$$h = -\phi_{1R}^0 s_\alpha + \phi_{2R}^0 c_\alpha, \quad (13)$$

where

$$\tan 2\alpha = \frac{2m_{12}}{m_{11} - m_{22}}, \quad (14)$$

and

$$m_{H,h}^2 = \frac{1}{2} \left(m_{11} + m_{22} \pm \sqrt{(m_{11} - m_{22})^2 + 4m_{12}^2} \right). \quad (15)$$

B. The Yukawa sector in the 2HDM-III with a four-zero texture

We shall follow Refs. [28, 33], where a specific four-zero texture has been implemented for the Yukawa matrices within the 2HDM-III. This allows one to express the couplings of the neutral and charged Higgs bosons in terms of the fermion masses, Cabibbo-Kobayashi-Maskawa (CKM) mixing angles and certain dimensionless parameters, which are to be bounded by current experimental constraints. The Yukawa Lagrangian is written as follows:

$$\mathcal{L}_Y = Y_1^u \bar{Q}_L \tilde{\Phi}_1 u_R + Y_2^u \bar{Q}_L \tilde{\Phi}_2 u_R + Y_1^d \bar{Q}_L \Phi_1 d_R + Y_2^d \bar{Q}_L \Phi_2 d_R + H.c., \quad (16)$$

where $\Phi_{1,2} = (\phi_{1,2}^+, \phi_{1,2}^0)^T$ refer to the two Higgs doublets, $\tilde{\Phi}_{1,2} = i\sigma_2 \Phi_{1,2}^*$, Q_L denotes the left-handed quark doublet, u_R and d_R are the right-handed quarks singlets, and $Y_{1,2}^{u,d}$ denotes the (3×3) Yukawa matrices. The Yukawa lepton sector is given by a similar expression.

Since the fermionic contribution to the one-loop reactions $\gamma\gamma \rightarrow \phi_i \phi_j$ is given by vertices $ff\phi_i$ involving only neutral Higgs bosons, we will concentrate only in this part of the Yukawa sector. After implementing the

diagonalizations carried out in the Higgs potential and in the Yukawa sector⁴, the interactions of the neutral Higgs bosons (h^0, H^0, A^0) with quark pairs acquire the following form:

$$\begin{aligned}
\mathcal{L}_Y^q = & \frac{g}{2} \left(\frac{m_{d_i}}{m_W} \right) \bar{d}_i \left[\frac{\cos \alpha}{\cos \beta} \delta_{ij} + \frac{\sqrt{2} \sin(\alpha - \beta)}{g \cos \beta} \left(\frac{m_W}{m_{d_i}} \right) (\tilde{Y}_2^d)_{ij} \right] d_j H^0 \\
& + \frac{g}{2} \left(\frac{m_{d_i}}{m_W} \right) \bar{d}_i \left[-\frac{\sin \alpha}{\cos \beta} \delta_{ij} + \frac{\sqrt{2} \cos(\alpha - \beta)}{g \cos \beta} \left(\frac{m_W}{m_{d_i}} \right) (\tilde{Y}_2^d)_{ij} \right] d_j h^0 \\
& + \frac{ig}{2} \left(\frac{m_{d_i}}{m_W} \right) \bar{d}_i \left[-\tan \beta \delta_{ij} + \frac{\sqrt{2}}{g \cos \beta} \left(\frac{m_W}{m_{d_i}} \right) (\tilde{Y}_2^d)_{ij} \right] \gamma^5 d_j A^0 \\
& + \frac{g}{2} \left(\frac{m_{u_i}}{m_W} \right) \bar{u}_i \left[\frac{\sin \alpha}{\sin \beta} \delta_{ij} - \frac{\sqrt{2} \sin(\alpha - \beta)}{g \sin \beta} \left(\frac{m_W}{m_{u_i}} \right) (\tilde{Y}_1^u)_{ij} \right] u_j H^0 \\
& + \frac{g}{2} \left(\frac{m_{u_i}}{m_W} \right) \bar{u}_i \left[\frac{\cos \alpha}{\sin \beta} \delta_{ij} - \frac{\sqrt{2} \cos(\alpha - \beta)}{g \sin \beta} \left(\frac{m_W}{m_{u_i}} \right) (\tilde{Y}_1^u)_{ij} \right] u_j h^0 \\
& + \frac{ig}{2} \left(\frac{m_{u_i}}{m_W} \right) \bar{u}_i \left[-\cot \beta \delta_{ij} + \frac{\sqrt{2}}{g \sin \beta} \left(\frac{m_W}{m_{u_i}} \right) (\tilde{Y}_1^u)_{ij} \right] \gamma^5 u_j A^0,
\end{aligned} \tag{17}$$

where $i = 1, 2, 3$, with $d_1 = d, d_2 = s, d_3 = b, u_1 = u, u_2 = c, u_3 = t$. These couplings depend on the rotated matrices $\tilde{Y}_n^q = V_q Y_n^q V_q^\dagger$ ($n = 1$ when $q = u$, and $n = 2$ when $q = d$). Here V_q is the diagonalizing mass matrix. In order to evaluate \tilde{Y}_n^q we need to focus in the quark mass matrix, which is given by,

$$M^q = \frac{1}{\sqrt{2}} (v_1 Y_1^q + v_2 Y_2^q), \quad (q = u, d). \tag{18}$$

We shall consider that all Yukawa matrices have the Hermitian four-zero texture form [31], and the quark masses have the same form, which are given by:

$$M^q = \begin{pmatrix} 0 & C_q & 0 \\ C_q^* & \tilde{B}_q & B_q \\ 0 & B_q^* & A_q \end{pmatrix} \quad (q = u, d). \tag{19}$$

This is called a four-zero texture because one assumes that the Yukawa matrices are Hermitian, therefore each u and d type Yukawa matrix contains two independent zeros. According to current analysis this type of texture satisfies the experimental constraints (i.e. the Flavor Violating Higgs interaction) and at the same time it permits to derive analytical expressions for the Higgs boson fermion couplings [28, 29, 30, 33, 34].

To diagonalize these mass matrices, we use the matrix V_q ⁵ in the following way:

$$\bar{M}^q = V_q M^q V_q^\dagger. \tag{20}$$

Following the analysis in [28] one can derive a better approximation for the product $V_q Y_n^q V_q^\dagger$, expressing the rotated matrix \tilde{Y}_n^q , in the form

$$[\tilde{Y}_n^q]_{ij} = \frac{\sqrt{m_i^q m_j^q}}{v} [\tilde{\chi}_n^q]_{ij} = \frac{\sqrt{m_i^q m_j^q}}{v} [\chi_n^q]_{ij} e^{i\vartheta_{ij}^q}, \tag{21}$$

where χ 's are unknown dimensionless parameters of the model, they come from the election of a specific texture of the Yukawa matrices. In order to perform our phenomenological study, we find it convenient to rewrite the Lagrangian

⁴ The details of both diagonalizations are presented in Ref. [28].

⁵ V_q is built as a product of two matrices O_q and P_q in the form $V_q = O_q^T P_q$. These matrices are given in [31].

given in Eq. (17) in terms of the coefficients $[\tilde{\chi}_n^q]_{ij}$, as follows:

$$\begin{aligned}
\mathcal{L}_Y^q = & \frac{g}{2} \bar{d}_i \left[\left(\frac{m_{d_i}}{m_W} \right) \frac{\cos \alpha}{\cos \beta} \delta_{ij} + \frac{\sin(\alpha - \beta)}{\sqrt{2} \cos \beta} \left(\frac{\sqrt{m_{d_i} m_{d_j}}}{m_W} \right) \tilde{\chi}_{ij}^d \right] d_j H^0 \\
& + \frac{g}{2} \bar{d}_i \left[- \left(\frac{m_{d_i}}{m_W} \right) \frac{\sin \alpha}{\cos \beta} \delta_{ij} + \frac{\cos(\alpha - \beta)}{\sqrt{2} \cos \beta} \left(\frac{\sqrt{m_{d_i} m_{d_j}}}{m_W} \right) \tilde{\chi}_{ij}^d \right] d_j h^0 \\
& + \frac{ig}{2} \bar{d}_i \left[- \left(\frac{m_{d_i}}{m_W} \right) \tan \beta \delta_{ij} + \frac{1}{\sqrt{2} \cos \beta} \left(\frac{\sqrt{m_{d_i} m_{d_j}}}{m_W} \right) \tilde{\chi}_{ij}^d \right] \gamma^5 d_j A^0. \\
& \frac{g}{2} \bar{u}_i \left[\left(\frac{m_{u_i}}{m_W} \right) \frac{\sin \alpha}{\sin \beta} \delta_{ij} - \frac{\sin(\alpha - \beta)}{\sqrt{2} \sin \beta} \left(\frac{\sqrt{m_{u_i} m_{u_j}}}{m_W} \right) \tilde{\chi}_{ij}^u \right] u_j H^0 \\
& + \frac{g}{2} \bar{u}_i \left[\left(\frac{m_{u_i}}{m_W} \right) \frac{\cos \alpha}{\sin \beta} \delta_{ij} - \frac{\cos(\alpha - \beta)}{\sqrt{2} \sin \beta} \left(\frac{\sqrt{m_{u_i} m_{u_j}}}{m_W} \right) \tilde{\chi}_{ij}^u \right] u_j h^0 \\
& + \frac{ig}{2} \bar{u}_i \left[- \left(\frac{m_{u_i}}{m_W} \right) \cot \beta \delta_{ij} + \frac{1}{\sqrt{2} \sin \beta} \left(\frac{\sqrt{m_{u_i} m_{u_j}}}{m_W} \right) \tilde{\chi}_{ij}^u \right] \gamma^5 u_j A^0.
\end{aligned} \tag{22}$$

where we have redefined $[\tilde{\chi}_1^u]_{ij} = \tilde{\chi}_{ij}^u$ and $[\tilde{\chi}_2^d]_{ij} = \tilde{\chi}_{ij}^d$. As it was discussed in Ref. [28], most low-energy processes imply weak bounds on the coefficients $\tilde{\chi}_{ij}^q$, which turn out to be of $O(1)$. Based on the analysis of $B \rightarrow X_s \gamma$ [52, 53], we find the bounds: $|\chi_{33}^{u,d}| \lesssim 1$ for $0.1 < \tan \beta \leq 70$ [30]. Other constraints on the charged Higgs mass and $\tan \beta$, can be obtained from anomalous magnetic moment of the muon Δa_μ , the ρ parameter, as well as B-decays into the tau lepton [54, 55]. For instance, as it can be read from Ref. [56], one has that the decay $B \rightarrow \tau \nu$, implies a constraint such that for $m_{H^+} = 200$ (300) GeV, values of $\tan \beta$ less than about 30 (50) are still allowed, within MSSM or THDM-II. However, these constraints can only be taken as estimates, as it is likely that they would be modified for THDM-III. A more detailed analysis that includes the most recent data is underway [57, 58]. On the other hand, the condition $\frac{\Gamma_{H^+}}{m_{H^+}} < \frac{1}{2}$ in the frame of the 2HDM-II implies $\frac{\Gamma_{H^+}}{m_{H^+}} \approx \frac{3G_F m_t^2}{4\sqrt{2}\pi \tan \beta^2}$ which leads to $0.3 \lesssim \tan \beta \lesssim 130$.

However, we found that in 2HDM-III $\frac{\Gamma_{H^+}}{m_{H^+}} \approx \frac{3G_F m_t^2}{4\sqrt{2}\pi \tan \beta^2} \left(\frac{1}{1 - \frac{\chi_{33}^u}{\sqrt{2} \cos \beta}} \right)^2$ [30], we have checked numerically that this leads to $0.08 < \tan \beta < 200$ when $|\chi_{33}^u| \approx 1$ and $0.3 < \tan \beta < 130$ as long as $|\tilde{\chi}_{33}^u| \rightarrow 0$ recovering the result for the case of the 2HDM-II [13, 59].

Other important bounds on $|\tilde{\chi}_{33}|$ and $\tan \beta$ come from radiative corrections to the process $\Gamma(Z \rightarrow b\bar{b})$, specially the hadronic branching fraction of Z bosons to $b\bar{b}$ (R_b) and the b quark asymmetry (A_b) imposed a high restriction [34, 60]. We can get bounds for $\tan \beta$: in the case $\chi_{33}^{u,d} = 1$ and $m_{H^+} \sim 200(300)$ GeV, the range $\tan \beta > 0.3(0.2)$ is allowed, while in the scenario $\chi_{33}^{u,d} = -1$ and $m_{H^+} \sim 200(300)$ GeV, $\tan \beta > 5(3)$ is permitted.

On the other hand, the leading contribution to $B_0 - \bar{B}_0$ mixing in the regime small $\tan \beta$ is given by the charged Higgs sector. Following the Ref. [34, 54], we get for the case $\chi_{33}^{u,d} = 1$ and $m_{H^+} \sim 200(300)$ GeV, $\tan \beta > 0.2(0.25)$ is allowed. Combining the criteria of the analysis for the radiative corrections of $Zb\bar{b}$ vertex and $B_0 - \bar{B}_0$ mixing, $\tan \beta > 0.3$ is allowed for $m_{H^+} > 170$ GeV and $\chi_{33}^{u,d} = 1$. However, when $\chi_{33}^{u,d} = -1$ and $m_{H^+} < 600$ GeV, $\tan \beta < 2$ is disfavored.

Besides, following the analysis of the Ref. [12, 34, 54], one can get the deviation $\Delta \rho_0$ of the parameter $\rho_0 = M_W^2 / \rho M_Z^2 C_W^2$ of our version 2HDM-III, where the ρ in the denominator absorbs all the SM corrections, and the most important SM correction at 1-loop level comes from the heavy top-quark. According the reported value of ρ_0 is [61]

$$\rho_0 = 1.004 \stackrel{+0.0027}{-0.0007} \quad (2\sigma). \tag{23}$$

In terms of new physics (2HDM-III) the constraint becomes:

$$-0.0007 < \Delta \rho_{2\text{HDM-III}} < 0.0027. \tag{24}$$

In 2HDM ρ_0 receives contribution from the Higgs bosons given by, in the context of model III [12, 54]

$$\begin{aligned}
\Delta \rho_{2\text{HDM-III}} = & \frac{G_F}{8\sqrt{2}\pi^2} \left[\sin^2(\alpha - \beta) F(M_{H^\pm}, M_A, M_{H^0}) \right. \\
& \left. + \cos^2(\alpha - \beta) F(M_{H^\pm}, M_A, M_{h^0}) \right],
\end{aligned} \tag{25}$$

where

$$F(m_1, m_2, m_3) = m_1^2 - \frac{m_1^2 m_2^2}{m_1^2 - m_2^2} \log\left(\frac{m_1^2}{m_2^2}\right) - \frac{m_1^2 m_3^2}{m_1^2 - m_3^2} \log\left(\frac{m_1^2}{m_3^2}\right) + \frac{m_2^2 m_3^2}{m_2^2 - m_3^2} \log\left(\frac{m_3^2}{m_2^2}\right).$$

Since ρ_0 is constrained to be around 1 we have to minimize the contributions of $\Delta\rho_{2\text{HDM-III}}$. This is obtained for the case $\alpha = 0, \pi/2$, and the parameter space of the scalar sector is strongly reduced when decoupling between Higgs bosons, i.e. $\Delta m_{ij} = m_i - m_j > 100$ GeV ($m_i = m_{h^0}, m_{H^0}, m_{A^0}, m_{H^\pm}$). However, is possible to avoid the constraint for $\Delta\rho_{2\text{HDM-III}}$ if the decoupling source $\Delta m_{ij} \sim 20$ GeV or $\Delta m_{ij} \sim 100$ GeV and one Higgs very heavy (e.g. $m_{H^0} > 1$ TeV). When $\alpha = \beta \pm \pi/2$ the allowed parameter region is larger and one can avoid the constraints of the ρ parameter with or without decoupling. Another interesting possibility is when we have the case quasi-degenerate between the masses of CP-even Higgs boson (H) and the charged Higgs boson (H^\pm). The reason is that, in a 2HDM, the custodial symmetry may be implemented either with $m_A = m_{H^\pm}$ or with $m_H = m_{H^\pm}$ [62]. The full study of the ρ parameter in our version 2HDM-III will be presented elsewhere [57].

Hereafter, we shall refer to three benchmark scenarios, namely:

- **Scenario I (the decoupling limit).** In this scenario, h assumes the role of the SM Higgs boson h_{SM} and is essentially independent from the diverse versions of the model. We have chosen to discuss the $\gamma\gamma \rightarrow hh$ process within this context to illustrate the decoupling nature of the heavy Higgs effects [50]. We will take $m_h = 120$ GeV and $m_A \sim m_{H^\pm} \sim m_H \gg v$. Two cases will be considered, one when the parameter of the Higgs potential μ_{12} is of the order of the Fermi scale, $\mu_{12} \sim v$, and other when this parameter is much larger than such scale, $\mu_{12} \gg v$.
- **Scenario II (SM-like)** [50]. This is a scenario of the 2HDM-III in which the couplings hVV ($V = W, Z$), hhh , $hhhh$ are nearly indistinguishable from the corresponding h_{SM} , whereas the hff couplings can deviate significantly from the corresponding $h_{SM}ff$ ones. We will take the following values for the parameters of the model $m_h = 120$ GeV, $m_A = 110$ GeV, $\mu_{12} = 130$ GeV, $m_{H^\pm} \sim m_H \sim m_A + m_h$ GeV, and $\alpha = \beta \pm \pi/2$. Within the two subscenarios: ($\lambda_7 = -\lambda_6 = -0.1$) and ($\lambda_7 = -\lambda_6 = -1$).
- **Scenario III (a more general case of 2HDM-III).** In this scenario, more general couplings of neutral Higgs bosons to SM particles are assumed. We will include the contributions of the parameters of the Higgs potential λ_6 and λ_7 , as well as the contributions of the Yukawa texture in the couplings $\phi f \bar{f}$. Within this scenario, a degenerate case, a nondegenerate case and the case with a light CP-odd scalar will be considered. In the nondegenerate case, we will choose $m_{H^\pm} = 400$ GeV, $m_A = 350$ GeV, $m_H = 520$ GeV, $m_h = 120$ GeV, and $\mu_{12} = 120$ GeV. On the other side, in the degenerate case we will choose $m_{H^\pm} = m_H = m_A = 300$ GeV, with $\mu_{12} = 60$ GeV and $m_h = 120$ GeV. For the case with light CP-odd scalar, we will choose $m_A = 50$ GeV, $m_h = 120$ GeV, $m_{H^\pm} = 350$ GeV, $m_H = 400$ GeV, and $\mu_{12} = 70$ GeV. In all cases, the $\alpha = \beta$ and $\alpha = \beta \pm \pi/2$ possibilities will be considered. In the nondegenerate case, the set of values $\lambda_7 = -\lambda_6 = -1$ and $\lambda_7 = -\lambda_6 = -0.1$ will be considered. As we will see below, only the values $\lambda_7 = -\lambda_6 = -1$ are relevant for the degenerate case and when we study the case with a light CP-odd scalar.

In all the above scenarios, we consider the constraints imposed by perturbativity, $Z \rightarrow b\bar{b}$, ρ_0 parameter, and $B^0 - \bar{B}^0$ mixing. Our predictions will be consistent with current bounds on the charged Higgs mass obtained at Tevatron [63] and LEP2 [61, 64], as well as with those derived theoretically [65].

III. THE GAUGE-FIXING PROCEDURE

As already mentioned, in calculating the $\gamma\gamma \rightarrow \phi_i \phi_j$ reaction we will define the W gauge boson propagator using a nonlinear gauge-fixing procedure that is covariant under the electromagnetic gauge group and consistent with renormalization theory. The details of this gauge-fixing procedure for the 2HDM has been reported recently in [44]. Here, we present the gauge-fixing functions, including some results and comments that are needed in calculating the amplitude for the $\gamma\gamma \rightarrow \phi_i \phi_j$ process.

To begin with, we discuss the most general structure of gauge-fixing functions f^a and f for the $SU_L(2)$ and $U_Y(1)$ gauge groups that are allowed by renormalization theory and covariance under the electromagnetic gauge group in the context of the 2HDM. As it is stressed in Ref.[44], our main aim is to remove the most nonphysical vertices that

are generated by the Higgs kinetic-energy term. This is achieved by introducing the following nonlinear gauge-fixing functions [44]:

$$f^a = f_V^a + f_S^a, \quad (26)$$

$$f = f_V + f_S, \quad (27)$$

where

$$f_V^a = \left(\delta^{ab} \partial_\mu - g' \epsilon^{3ab} B_\mu \right) W^{b\mu}, \quad (28)$$

$$f_S^a = \frac{ig\xi}{2} \left\{ \sum_{i=1}^2 \left[\Phi_i^\dagger (\sigma^a - i\epsilon^{3ab} \sigma^b) \Phi_{0i} - \Phi_{0i}^\dagger (\sigma^a + i\epsilon^{3ab} \sigma^b) \Phi_i \right] + i\epsilon^{3ab} (c_\beta \Phi_1^\dagger + s_\beta \Phi_2^\dagger) \sigma^b (c_\beta \Phi_1 + s_\beta \Phi_2) \right\}, \quad (29)$$

and

$$f_V = \partial_\mu B^\mu, \quad (30)$$

$$f_S = \frac{ig'\xi}{2} \sum_{i=1}^2 \left(\Phi_i^\dagger \Phi_{0i} - \Phi_{0i}^\dagger \Phi_i \right). \quad (31)$$

In the above expressions, $\Phi_{0i}^\dagger = (0, v_i/\sqrt{2})$, σ^a are the Pauli matrices, and W_μ^a and B_μ are the gauge fields associated with the electroweak group. Our gauge-fixing functions contain the conventional linear functions as a particular case, which are obtained when ϵ^{3ab} is set to zero. Also, it is worth mentioning that this gauge-fixing procedure contains as a particular case an analogous gauge scheme for the minimal SM [46], which becomes evident when the Φ_1 doublet is associated with the SM one and β is set to zero.

To fully appreciate the structure of the gauge-fixing functions, it is convenient to express them in terms of mass eigenstates fields. After this, one obtains for the vector sector

$$f_V^+ = \bar{D}_\mu W^{+\mu}, \quad (32)$$

$$f_V^Z = \partial_\mu Z^\mu, \quad (33)$$

$$f_V^A = \partial_\mu A^\mu, \quad (34)$$

and for the scalar sector

$$f_S^+ = -\frac{ig\xi}{2} (\varphi^0 - iG_Z) G_W^+, \quad (35)$$

$$f_S^Z = -\xi m_Z G_Z, \quad (36)$$

$$f_S^A = 0, \quad (37)$$

where $\varphi^0 = v + c_{\beta-\alpha} H + s_{\beta-\alpha} h$ and $\bar{D}_\mu = \partial_\mu - ig' B_\mu$, being g' the coupling constant associated with the $U_Y(1)$ group. We can see that both f_V^+ and f_S^+ are nonlinear and transform covariantly under the $U_e(1)$ group, as \bar{D}_μ contains the covariant derivative associated with this group.

Following the study of Ref. [44], the gauge-fixing Lagrangian, \mathcal{L}_B , can then be written as

$$\mathcal{L}_B = \mathcal{L}_{BV} + \mathcal{L}_{BS} + \mathcal{L}_{BSV}, \quad (38)$$

where

$$\mathcal{L}_{BV} = -\frac{1}{\xi} (\bar{D}_\mu W^{+\mu})^\dagger (\bar{D}_\nu W^{+\nu}) - \frac{1}{2\xi} (\partial_\mu Z^\mu)^2 - \frac{1}{2\xi} (\partial_\mu A^\mu)^2, \quad (39)$$

$$\mathcal{L}_{BS} = -\frac{g^2\xi}{4} (\varphi^2 + G_Z^2) G_W^- G_W^+ - \frac{1}{2}\xi m_Z^2 G_Z^2, \quad (40)$$

$$\mathcal{L}_{BSV} = \frac{ig}{2} \left[(\bar{D}_\mu W^{+\mu})^\dagger (\varphi - iG_Z) G_W^+ - (\bar{D}_\mu W^{+\mu}) (\varphi + iG_Z) G_W^- \right] + m_Z G_Z \partial_\mu Z^\mu. \quad (41)$$

We restrict our discussion to present some comments concerning the impact of the \mathcal{L}_{BV} , \mathcal{L}_{BS} , and \mathcal{L}_{BSV} Lagrangians on the Yang–Mills, the Higgs kinetic–energy, and the Higgs potential sectors, respectively. First of all, the term \mathcal{L}_{BV} defines the propagators of the gauge fields and also modifies nontrivially the Lorentz structure of the trilinear and quartic vertices arising from the Yang–Mills sector. Indeed, with the exception of the $WWWW$ vertex, all trilinear and quartic vertices are modified by the gauge fixing procedure. Since the term that introduces the modifications on these vertices is invariant under the $U_e(1)$ group [44], the trilinear electromagnetic vertices satisfy QED-like Ward identities. This fact is relevant for radiative corrections as such a symmetry greatly simplifies this class of calculations.

As for the \mathcal{L}_{BS} term, it defines the masses of the G_W and G_Z fields and modifies some nonphysical couplings arising from the Higgs potential. In this gauge, the couplings between scalar fields arise solely from the sum of the following terms $-V(\Phi_1, \Phi_2) + \mathcal{L}_{BS}$. The last term in this sum leads to modifications in the strength of the nonphysical couplings $HG_W^-G_W^+$, $hG_W^-G_W^+$, $H^2G_W^-G_W^+$, $h^2G_W^-G_W^+$, $HhG_W^-G_W^+$, and $G_Z^2G_W^-G_W^+$. The physical couplings remain unchanged, as required.

On the other hand, the term \mathcal{L}_{BSV} considerably affects the Higgs kinetic–energy sector of the theory since it removes several nonphysical vertices. When these two terms are combined, one finds [44] that not only the mixing terms $W - G_W$ and $Z - G_Z$ are removed from the theory, as it occurs in conventional linear gauges, but also the nonphysical vertices $WG_W\gamma$, WG_WZ , $HWG_W\gamma$, $hWG_W\gamma$, $G_ZWG_W\gamma$, HWG_WZ , hWG_WZ , and G_ZWG_WZ are removed. In addition, the unphysical vertices HWG_W , hWG_W , and G_ZWG_W are modified. Once again, it should be emphasized that the couplings involving only physical scalars are not modified by the gauge-fixing procedure.

As far as the ghost sector is concerned, it is shown in Ref. [44] that it shows new interesting aspects that are not present in conventional linear gauges, such as manifest electromagnetic gauge invariance and the presence of quartic ghost interactions. As a consequence of $U_e(1)$ –gauge invariance, the corresponding electromagnetic couplings satisfy QED-like Ward identities, which considerably simplifies the loop calculations associated with the $\gamma\gamma \rightarrow \phi_i\phi_j$ process.

The gauge-dependent Feynman rules necessary for the calculation of the $\gamma\gamma \rightarrow \phi_i\phi_j$ processes are not presented here, as they are given in Ref. [44]. The rest of Feynman rules, which do not depend of the gauge-fixing procedure, are given in an Appendix A.

IV. THE PROCESSES $\gamma\gamma \rightarrow \phi_i\phi_j$

We now will exploit the nonlinear R_ξ –gauge already introduced to calculate the $\gamma\gamma \rightarrow \phi_i\phi_j$ process. To begin with, we would like to discuss the basics of this process, such as its kinematics and the gauge structure dictated by electromagnetic gauge invariance. To this end, we use the following notation:

$$A_\mu(k_1) + A_\nu(k_2) \rightarrow \phi_i(k_3) + \phi_j(k_4), \quad (42)$$

where the particle momenta satisfy the kinematic relation $k_1 + k_2 = k_3 + k_4$. The Mandelstam variables associated with this process are $s = (k_1 + k_2)^2$, $t = (k_2 - k_3)^2$, and $u = (k_1 - k_3)^2$, which fulfill the relationship $s + t + u = k_3^2 + k_4^2$. One useful quantity is the transversal momentum, given by

$$k_T^2 = \frac{1}{s}(tu - k_3^2 k_4^2). \quad (43)$$

As far as the gauge structures are concerned, two possibilities arise depending on the CP properties of the final particles. One possibility corresponds to final states with two Higgs particles both CP–even, i.e. $\phi_a\phi_a$ or both CP–odd, AA . Although it is possible to construct at least three gauge electromagnetic structures, only two of them are independent. We find it convenient to use the following basis:

$$P_{1\mu\nu} = \frac{\sqrt{2}}{s} \left(k_{2\mu} k_{1\nu} - k_1 \cdot k_2 g_{\mu\nu} \right), \quad (44)$$

$$P_{2\mu\nu} = \frac{\sqrt{2}}{k_T^2 s} \left[\frac{1}{2} k_T^2 s g_{\mu\nu} + k_3^2 k_{2\mu} k_{1\nu} - 2k_2 \cdot k_3 k_{3\mu} k_{1\nu} - 2k_1 \cdot k_3 k_{2\mu} k_{3\nu} + 2k_1 \cdot k_2 k_{3\mu} k_{3\nu} \right], \quad (45)$$

which is orthonormal in the sense that $P_i^{\mu\nu} P_{j\mu\nu} = \delta_{ij}$. Another possibility corresponds to final particles with distinct CP properties, i.e., $A\phi_a$. The corresponding gauge structures can be assembled by combining the Levi-Civita tensor and the 4-vectors $k_{1\mu}$, $k_{2\mu}$, and $k_{3\mu}$. However, not all the combinations are independent as some of them can be eliminated with the help of Schouten’s identity. Once those redundant structures are removed, we are left with two

independent gauge structures. We choose the following basis

$$\tilde{P}_{1\mu\nu} = \frac{\sqrt{2}}{s} \epsilon_{\mu\nu\alpha\beta} k_1^\alpha k_2^\beta, \quad (46)$$

$$\tilde{P}_{2\mu\nu} = \frac{2\sqrt{2}}{k_T^2 s} \left[\frac{1}{2} k_3^2 \epsilon_{\mu\nu\alpha\beta} k_1^\alpha k_2^\beta + k_1 \cdot k_3 \epsilon_{\mu\nu\alpha\beta} k_2^\alpha k_3^\beta + k_{3\mu} \epsilon_{\nu\alpha\beta\gamma} k_1^\alpha k_2^\beta k_3^\gamma \right], \quad (47)$$

which also are orthonormal. The invariant amplitude can be written as follows:

$$\mathcal{M} = \mathcal{M}_{\mu\nu} \epsilon^\mu(k_1, \lambda_1) \epsilon^\nu(k_2, \lambda_2), \quad (48)$$

where $\epsilon^\mu(k_1, \lambda_1)$ and $\epsilon^\nu(k_2, \lambda_2)$ are the polarization vectors of the photons. The tensor amplitude reads

$$\mathcal{M}_{\mu\nu} = \frac{\alpha^2}{\sqrt{2} s_W^2} \begin{cases} A_1 P_{1\mu\nu} + A_2 P_{2\mu\nu} & \text{for } AA, \phi_a \phi_a, \\ \tilde{A}_1 \tilde{P}_{1\mu\nu} + \tilde{A}_2 \tilde{P}_{2\mu\nu} & \text{for } A\phi_a \end{cases}, \quad (49)$$

and the unpolarized cross-section for the process $\gamma\gamma \rightarrow \phi_i \phi_i$ is given by

$$\begin{aligned} \sigma(\gamma\gamma \rightarrow \phi_i \phi_i) &= \frac{1}{16\pi s^2 \epsilon} \int_{t_1}^{t_0} dt \sum_{spin} |\mathcal{M}|^2 \\ &= \frac{\alpha^4}{128\pi s_W^4 s^2 \epsilon} \int_{t_1}^{t_0} dt \begin{cases} (|A_1|^2 + |A_2|^2), \\ (|\tilde{A}_1|^2 + |\tilde{A}_2|^2), \end{cases} \end{aligned} \quad (50)$$

where $\epsilon = 2$ if the final particles are identical and 1 otherwise. The integration limits are

$$t_0(t_1) = -\frac{s}{2} \left[1 - \frac{k_3^2 + k_4^2}{s} \mp \sqrt{1 - 2\left(\frac{k_3^2 + k_4^2}{s}\right) + \left(\frac{k_3^2 - k_4^2}{s}\right)^2} \right]. \quad (51)$$

We will present below the amplitudes for the three available processes: $\gamma\gamma \rightarrow AA$, $\gamma\gamma \rightarrow A\phi_a$, and $\gamma\gamma \rightarrow \phi_a \phi_b$. The absence of the unphysical $\gamma W G_W$ and $\phi_a \gamma W G_W$ vertices⁶ introduces considerable simplifications in the calculations. In particular, there are a significant reduction in the number of diagrams with respect to those appearing in a linear gauge. Also, the contributions can be grouped into distinct sets of diagrams which lead to finite and gauge invariant results by their own (see Figs. 1-5).

We find it convenient to express our results in terms of Passarino-Veltman scalar functions. For those scalar functions arising from the sets of diagrams of Figs. 1 through 4, an unambiguous shorthand notation can be used:

$$C_0(a, b) = C_0(k_a^2, k_b^2, (k_a + k_b)^2, m^2, m^2, m^2), \quad (52)$$

$$D_0(a, b, c) = D_0(k_a^2, k_b^2, k_c^2, (k_a + k_b + k_c)^2, (k_a + k_b)^2, (k_b + k_c)^2, m^2, m^2, m^2), \quad (53)$$

where the right-hand side has been expressed in the notation of Ref. [66]. In addition, a , b , and c run over 1 to 3, and m is the mass of the particle circulating in the loop. Below it will be evident why it is not necessary to specify m as an argument of the scalar functions. Unfortunately this scheme cannot be used for the scalar functions arising from Fig. 5 since two different particles circulate in the loop, so an adequate notation for these scalar functions will be given below.

It is also convenient to introduce the following dimensionless variables $x_f = m_f^2/s$, $x_A = m_A^2/s$, $x_a = m_a^2/s$ (m_a stands for the mass of ϕ_a), $x_H = m_{H^\pm}^2/s$, $x_W = m_W^2/s$, $x_T = k_T^2/s$, $x_t = t/s$, $x_u = u/s$, and $\gamma_i = \Gamma_i/\sqrt{s}$, being Γ_i the total width of ϕ_i .

A. The process $\gamma\gamma \rightarrow AA$

This process receives contributions from charged fermions, the W gauge boson and the charged Higgs boson H^\pm . These contributions arise through the diagrams shown in Figs. 1, 2, 3, and 5. There are not contributions from

⁶ The $A\gamma W G_W$ vertex is not generated by the theory.

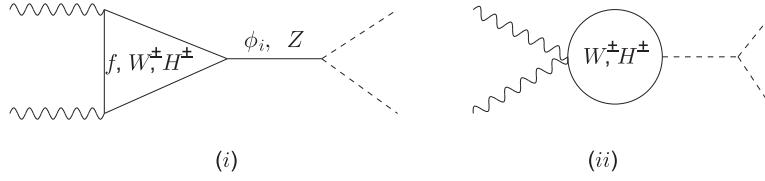


FIG. 1: Feynman diagrams contributing to the $\gamma\gamma \rightarrow \phi_i\phi_j$ processes in the nonlinear gauge, in which this contribution is ultraviolet finite and gauge invariant by itself. In the case of the W contribution, similar diagrams are to be considered for the pseudo-Goldstone and ghost fields. Crossed diagrams are not shown.



FIG. 2: The same as in Fig. 1.

diagrams of Fig. 4 since the AWG_W vertex is not generated by the theory. As pointed out before, in the nonlinear gauge, each set of diagrams leads to an ultraviolet finite and gauge invariant amplitude. All of the diagrams of Figs. 1, 2, 3, and 5 contribute to the A_1 amplitude, but only the diagrams of Figs. 3 and 5 contribute to A_2 . These contributions can conveniently written as:

$$A_1 = A_{11} + A_{12} + A_{13} + A_{15}, \quad (54)$$

$$A_2 = A_{23} + A_{25}, \quad (55)$$

where the subscript j in A_{ij} denotes the contributions coming from each set of diagrams, which can be expressed in terms of the contributions of each kind of particles circulating in the loops as follows:

$$A_{11} = F_{11} + S_{11} + G_{11}, \quad (56)$$

$$A_{12} = S_{12} + G_{12}, \quad (57)$$

$$A_{13} = F_{13}, \quad (58)$$

$$A_{23} = F_{23}, \quad (59)$$

where we will use the letters F_{ij} , S_{ij} , and G_{ij} to denote the contributions coming from fermion, scalar, and gauge particles, respectively. The set of diagrams in Fig. 1 yield

$$F_{11} = - \sum_f N_f Q_f^2 \sum_{\phi_a} (\mathcal{G}_{\phi_a \bar{f} f} \mathcal{G}_{\phi_a A A}) \frac{x_f}{1 - x_a + i\sqrt{x_a} \gamma_a} [2 + (4x_f - 1)sC_0(1, 2)], \quad (60)$$

$$S_{11} = - \sum_{\phi_a} \left(\frac{\mathcal{G}_{\phi_a H^- H^+} \mathcal{G}_{\phi_a A A}}{4} \right) \frac{x_W}{1 - x_a + i\sqrt{x_a} \gamma_a} [1 + 2x_H sC_0(1, 2)], \quad (61)$$

$$G_{11} = - \sum_{\phi_a} \left(\frac{\mathcal{G}_{\phi_a W W} \mathcal{G}_{\phi_a A A}}{2} \right) \frac{x_W}{1 - x_a + i\sqrt{x_a} \gamma_a} \left[12 + \frac{x_a}{x_W} + (12x_W - 4 + x_a) 2sC_0(1, 2) \right], \quad (62)$$

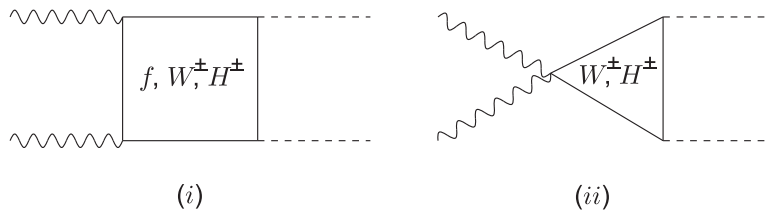


FIG. 3: The same as in Fig. 1.

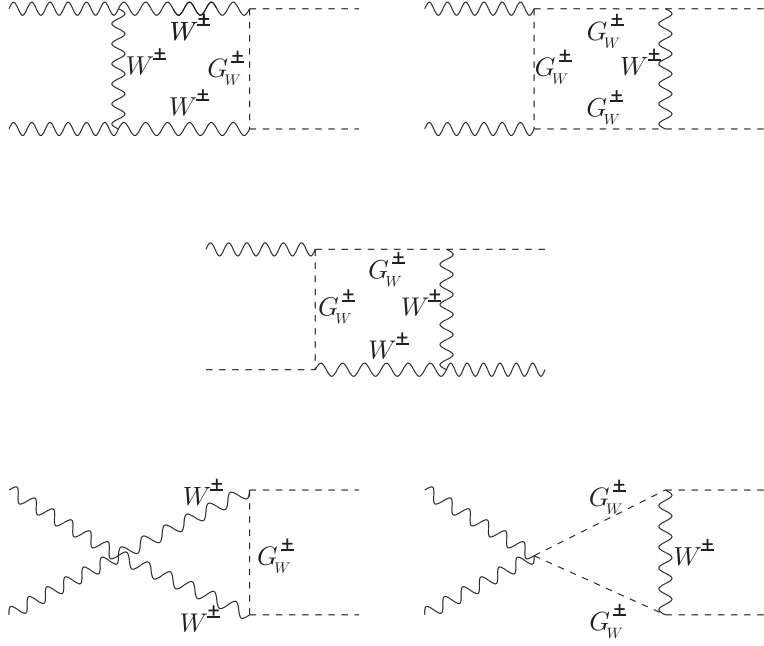


FIG. 4: Feynman diagrams contributing to the $\gamma\gamma \rightarrow \phi_i \phi_j$ processes in the nonlinear gauge. The contribution of these diagrams is finite and gauge invariant by itself. Crossed diagrams are not shown.

where N_f is the color index and Q_f is the electric charge in units of the positron charge, $\mathcal{G}_{\phi_a(ff,VV,\phi\phi)}$ are functions of the couplings $g_{\phi_a(ff,VV,\phi\phi)}$, which they are given in Appendix. Notice that there is no contribution from the one-loop $\gamma\gamma Z^*$ off-shell coupling [67] as the Z boson only couples to pairs of the form $A\phi_a$. In the set of diagrams of Fig. 2 there are only contributions from the charged scalar boson and the W gauge boson. The corresponding amplitudes are

$$S_{12} = -\left(\frac{\mathcal{G}_{H^\pm H^\mp AA}}{4}\right)[1 + 2x_H s C_0(1, 2)], \quad (63)$$

$$G_{12} = -8\left[1 - (1 - 2x_W)s C_0(1, 2) + \left(\frac{\mathcal{G}_{G_W^\pm G_W^\mp AA}}{32}\right)[1 + 2x_W s C_0(1, 2)]\right]. \quad (64)$$

There are contributions to G_{12} from the W boson and its associated pseudo-Goldstone boson, but not from the ghost field because of the absence of the $\bar{C}^\pm C^\mp AA$ vertex. As far as the diagrams of Fig. 3 is concerned, there are no contributions from scalar or gauge particles due to the absence of the $H^\pm H^\mp A$ and WWA vertices. The fermion contributions are given by

$$F_{13} = 2 \sum_f N_f Q_f^2 \mathcal{G}_{A\bar{f}f}^2 \left(\frac{x_f}{x_W}\right) \left\{ 2 + 4x_f s C_0(1, 2) + 2x_A s \left[(x_t - x_A) C_0(2, 3) + (x_u - x_A) C_0(1, 3) \right] + s^2 \left[-x_A x_T D_0(1, 3, 2) + x_f (1 - 2x_A) \left[D_0(1, 2, 3) + D_0(1, 3, 2) + D_0(2, 1, 3) \right] \right] \right\}, \quad (65)$$

$$F_{23} = 2 \sum_f N_f Q_f^2 \mathcal{G}_{A\bar{f}f}^2 \left(\frac{x_f}{x_W}\right) \left\{ s \left[C_0(1, 2) + (2x_A - 1) C_0(3, 4) + (x_t - x_A) C_0(2, 3) + (x_u - x_A) C_0(1, 3) + \frac{1 - 2x_A}{2x_T} \left[2x_t (x_t - x_A) C_0(2, 3) + 2x_u (x_u - x_A) C_0(1, 3) - (1 - 2x_A) C_0(1, 2) - (x_t - x_u)^2 C_0(3, 4) \right] + \frac{s^2}{2x_T} \left[-2(1 - 2x_A) x_f x_T \left[D_0(1, 2, 3) + D_0(1, 3, 2) + D_0(2, 1, 3) \right] + x_t (x_t^2 + x_A^2) D_0(1, 2, 3) + x_u (x_u^2 + x_A^2) D_0(2, 1, 3) \right] \right\}. \quad (66)$$

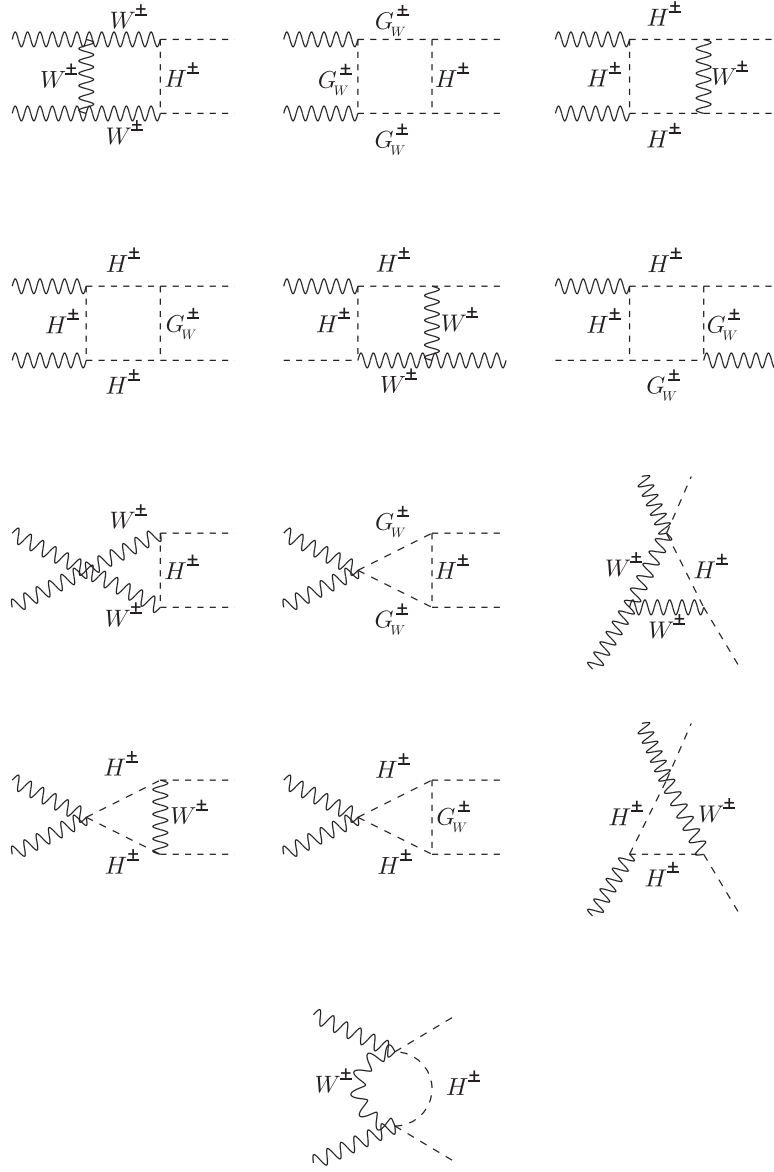


FIG. 5: The same as in Fig. 4.

Finally, the contributions from Fig. 5 read

$$A_{15} = 2 + s \sum_{a=3}^{12} f_a^1 C_0(a) + s^2 \sum_{a=1}^6 g_a^1 D_0(a), \quad (67)$$

$$A_{25} = \frac{1}{x_W x_T} \left[s \sum_{a=1}^{12} f_a^2 C_0(a) + s^2 \sum_{a=1}^6 g_a^2 D_0(a) \right], \quad (68)$$

where

$$f_3^1 = -4x_H, \quad (69)$$

$$f_4^1 = -8(1 - x_W), \quad (70)$$

$$f_5^1 = f_6^1 = f_{11}^1 = f_{12}^1 = \frac{1}{x_W} A_0(x_u - x_A), \quad (71)$$

$$f_7^1 = f_8^1 = f_9^1 = f_{10}^1 = \frac{1}{x_W} A_0(x_t - x_A), \quad (72)$$

$$g_1^1 = g_3^1 = -2\left(\frac{x_H}{x_W}\right)(2x_W + A_0), \quad (73)$$

$$g_2^1 = g_4^1 = -2(2x_H + A_0), \quad (74)$$

$$g_5^1 = g_6^1 = -4x_H - \frac{(x_T + x_H + x_W)A_0}{x_W}, \quad (75)$$

$$f_1^2 = f_2^2 = (2x_W + A_0)[2x_T + (x_t - x_u)^2], \quad (76)$$

$$f_3^2 = (2x_W + A_0)(2x_W - 2x_H - x_t - x_u) \quad (77)$$

$$f_4^2 = (2x_W + A_0)(2x_H - 2x_W - x_t - x_u) - 8x_T x_W; \quad (78)$$

$$f_5^2 = f_6^2 = f_{11}^2 = f_{12}^2 = (x_A - x_u)[x_u A_0 - 2x_W(x_A - x_u)^2], \quad (79)$$

$$f_7^2 = f_8^2 = f_9^2 = f_{10}^2 = f_5^2(x_u \rightarrow x_t), \quad (80)$$

$$g_1^2 = (A_0 + 2x_W)[2x_T x_H + (x_H + x_u - x_W)^2], \quad (81)$$

$$\begin{aligned} g_2^2 = & 4x_W(x_A - x_u)^4 - 4x_W(x_A - x_u)^3 + (x_A - x_u)^2[2(2x_A + 2x_H - 4x_W + 1)x_W + A_0(1 - 2x_W)] \\ & + 2(x_A - x_u)[2x_W(x_W - x_A) + A_0(x_H - x_A)] + A_0^2 + 2x_W(x_A + 1)A_0 + 4x_A x_H x_W, \end{aligned} \quad (82)$$

$$g_3^2 = g_1^2(x_u \rightarrow x_t), \quad (83)$$

$$g_4^2 = g_2^2(x_t \leftrightarrow x_u), \quad (84)$$

$$\begin{aligned} g_5^2 = g_6^2 = & \frac{1}{4} \left\{ (A_0 + 2x_W)(2x_H - 2x_W + x_t + x_u)^2 \right. \\ & + 2[A_0(x_T - x_t - x_u) - 2x_W(x_t + x_u)](2x_H - 2x_W + x_t + x_u) \\ & + 8x_T x_W(A_0 + 2x_W) + 8x_T^2 x_W - 2A_0(x_t + x_u)x_T \\ & \left. + (A_0 + 2x_W)(x_t + x_u)^2 \right\}. \end{aligned} \quad (85)$$

with

$$A_0 = x_A^2 - 2(x_H + x_W)x_A + (x_H - x_W)^2, \quad (86)$$

The arguments for the $C_0(a)$ and $D_0(a)$ scalar functions are presented in Appendix B.

B. The process $\gamma\gamma \rightarrow \phi_a \phi_b$

We turn now to the amplitudes associated with the final states hh , hH , and HH . There are contributions from all the sets of diagrams shown in Figs. 1 to 5. According to our notation, the contributions can be organized as follows:

$$A_1 = A_{11} + A_{12} + A_{13} + A_{14} + A_{15}, \quad (87)$$

$$A_2 = A_{23} + A_{24} + A_{25}, \quad (88)$$

where

$$A_{11} = F_{11} + S_{11} + G_{11}, \quad (89)$$

$$A_{12} = S_{12} + G_{12}, \quad (90)$$

$$A_{13} = F_{13} + S_{13} + G_{13}, \quad (91)$$

$$A_{23} = F_{23} + S_{23} + G_{23}. \quad (92)$$

The A_{14} , A_{15} , A_{24} , and A_{25} partial amplitudes only receive contributions from the pairs (W, G_W) and (W, H^\pm) . The contributions coming from the set of diagrams in Fig. 1 are given by

$$F_{11} = \sum_f N_f Q_f^2 \sum_{\phi_c} (\mathcal{G}_{\phi_c \bar{f} f} \mathcal{G}_{\phi_c \phi_b \phi_a}) \frac{x_f}{1 - x_c + i\sqrt{x_c} \gamma_c} [2 + (4x_f - 1)sC_0(1, 2)], \quad (93)$$

$$S_{11} = - \sum_{\phi_c} \left(\frac{\mathcal{G}_{\phi_c H^\pm H^\mp} \mathcal{G}_{\phi_c \phi_b \phi_a}}{4} \right) \frac{x_W}{1 - x_c + i\sqrt{x_c} \gamma_c} [1 + 2x_H sC_0(1, 2)], \quad (94)$$

$$G_{11} = - \sum_{\phi_c} \left(\frac{\mathcal{G}_{\phi_c WW} \mathcal{G}_{\phi_c \phi_b \phi_a}}{2} \right) \frac{x_W}{1 - x_c + i\sqrt{x_c} \gamma_c} \left[12 + \frac{x_c}{x_W} + 2(-4 + 12x_W + x_c)sC_0(1, 2) \right], \quad (95)$$

$$S_{12} = \frac{-\mathcal{G}_{H^\pm H^\mp \phi_a \phi_b}}{4} [1 + 2x_H sC_0(1, 2)], \quad (96)$$

$$G_{12} = 8sC_0(1, 2)\delta^{ab} + (2C_0(1, 2)sx_W + 1)(2\mathcal{G}_{\phi_a WW} \mathcal{G}_{\phi_b WW} - \frac{1}{4}\mathcal{G}_{G_W^\pm G_W^\mp \phi_a \phi_b} - 8\delta^{ab}), \quad (97)$$

$$\begin{aligned} F_{13} = & \sum_f N_f Q_f^2 (\mathcal{G}_{\phi_a \bar{f} f} \mathcal{G}_{\phi_b \bar{f} f}) \left(\frac{x_f}{x_W} \right) \left\{ 4 \left[1 + 2x_f sC_0(1, 2) \right] + \right. \\ & (1 + x_t + x_u - 8x_f)s \left[(x_u - x_a)C_0(1, 3) + (x_u - x_b)C_0(2, 4) + (x_t - x_a)C_0(2, 3) + (x_t - x_b)C_0(1, 4) \right] - \\ & 2x_f(1 + x_a + x_b - 8x_f)s^2 \left[D_0(1, 2, 3) + D_0(2, 1, 3) \right] + \\ & \left. \left[16x_f^2 + 2x_f(4x_T - x_a - x_b - 1) - x_T(x_a + x_b) \right] s^2 D_0(1, 3, 2) \right\}, \end{aligned} \quad (98)$$

$$\begin{aligned} S_{13} = & - \left(\frac{\mathcal{G}_{\phi_a H^\pm H^\mp} \mathcal{G}_{\phi_b H^\pm H^\mp}}{4} \right) x_W s \left\{ (x_a - x_u)C_0(1, 3) + (x_b - x_u)C_0(2, 4) + (x_a - x_t)C_0(2, 3) + \right. \\ & \left. (x_b - x_t)C_0(1, 4) + 2x_H s \left[D_0(1, 2, 3) + D_0(2, 1, 3) + D_0(1, 3, 2) \right] + x_T s D_0(1, 3, 2) \right\}, \end{aligned} \quad (99)$$

$$\begin{aligned} G_{13} = & \left(- \frac{\mathcal{G}_{\phi_a WW} \mathcal{G}_{\phi_b WW}}{x_W} \right) s \left\{ A_G \left[(x_a - x_u)C_0(1, 3) + (x_b - x_u)C_0(2, 4) + (x_a - x_t)C_0(2, 3) \right. \right. \\ & \left. \left. + (x_b - x_t)C_0(1, 4) \right] + 2x_W s (A_G - 4x_W) \left[D_0(1, 2, 3) + D_0(2, 1, 3) + D_0(1, 3, 2) \right] + \right. \\ & \left. s x_T A_G D_0(1, 3, 2) \right\}, \end{aligned} \quad (100)$$

with

$$A_G = 16x_W^2 + x_b x_a + 2x_W(x_a + x_b). \quad (101)$$

$$\begin{aligned}
A_{14} = & (4\mathcal{G}_{\phi_a WW}\mathcal{G}_{\phi_b WW})s \left\{ -2C_0(1,2) + \right. \\
& (x_a + x_b) \left[(x_a - x_u)C_0(1,3) + (x_b - x_u)C_0(2,4) + (x_a - x_t)C_0(2,3) + (x_b - x_t)C_0(1,4) \right] + \\
& \left. 2x_W(x_t + x_u)s \left[D_0(1,2,3) + D_0(2,1,3) + D_0(1,3,2) \right] + x_T(x_a + x_b)sD_0(1,3,2) \right\}, \quad (102)
\end{aligned}$$

$$A_{15} = \left(\mathcal{G}_{W^\pm H^\mp \phi_a} \mathcal{G}_{W^\pm H^\mp \phi_b} \right) \left[2 + s \sum_{a=3}^{12} f_a^1 C_0(a) + s^2 \sum_{a=1}^6 g_a^1 D_0(a) \right], \quad (103)$$

where

$$f_3^1 = -4x_H, \quad (104)$$

$$f_4^1 = 8(x_W - 1), \quad (105)$$

$$f_5^1 = f_6^1 = -(x_a - x_u)f, \quad (106)$$

$$f_7^1 = f_8^1 = -(x_a - x_t)f, \quad (107)$$

$$f_9^1 = f_{10}^1 = (x_b - x_t)f, \quad (108)$$

$$f_{11}^1 = f_{12}^1 = (x_b - x_u)f, \quad (109)$$

$$g_1^1 = g_3^1 = -2x_H(f + 2), \quad (110)$$

$$g_2^1 = g_4^1 = -2x_W \left(f + 2 \frac{x_H}{x_W} \right), \quad (111)$$

$$g_5^1 = g_6^1 = -(x_H + x_W + x_T)f - 4x_H x_W, \quad (112)$$

with

$$f = \frac{(x_H - x_W)^2 - (x_H + x_W)(x_a + x_b) + x_a x_b}{x_W}. \quad (113)$$

$$\begin{aligned}
F_{23} = & \sum_f N_f Q_f^2 (\mathcal{G}_{\phi_a \bar{f} f}) s \left\{ - \left[\frac{x_t^2 + x_u^2 - 8x_f(x_t + x_u) + 2x_a x_b}{x_T} \right] C_0(1,2) + \right. \\
& \left(\frac{x_t^2 + x_u^2 - 2x_a x_b}{x_T} \right) (x_t + x_u - 8x_f) C_0(3,4) + \\
& \left[\frac{x_t(x_t - 8x_f) + x_a x_b}{x_T} \right] \left[(x_a - x_t)C_0(2,3) + (x_b - x_t)C_0(1,4) \right] + \\
& \left[\frac{x_u(x_u - 8x_f) + x_a x_b}{x_T} \right] \left[(x_a - x_u)C_0(1,3) + (x_b - x_u)C_0(2,4) \right] + \\
& 2x_f(x_t + x_u - 8x_f)sD_0(1,3,2) + \\
& s \left[-16x_f^2 + 2x_f(x_t + x_u - 4\frac{x_t^2}{x_T}) + (x_t^2 + x_a x_b)\frac{x_t}{x_T} \right] D_0(1,2,3) + \\
& s \left[-16x_f^2 + 2x_f(x_t + x_u - 4\frac{x_u^2}{x_T}) + (x_u^2 + x_a x_b)\frac{x_u}{x_T} \right] D_0(2,1,3) \Big\}, \quad (114)
\end{aligned}$$

$$S_{23} = \left(\frac{\mathcal{G}_{\phi_a H^\pm H^\mp} \mathcal{G}_{\phi_b H^\pm H^\mp}}{4} \right) \left(\frac{x_W}{x_T} \right) s (A + x_H B) \quad (115)$$

$$G_{23} = (\mathcal{G}_{\phi_a WW} \mathcal{G}_{\phi_b WW}) \left(\frac{1}{x_T x_W} \right) A_G s (A + x_W B), \quad (116)$$

with A and B given by

$$A = -(x_t + x_u)C_0(1, 2) + (x_t^2 + x_u^2 - 2x_a x_b)C_0(3, 4) + x_t(x_a - x_t)C_0(2, 3) + x_t(x_b - x_t)C_0(1, 4) + x_u(x_a - x_u)C_0(1, 3) + x_u(x_b - x_u)C_0(2, 4) + s[x_t^2 D_0(1, 2, 3) + x_u^2 D_0(2, 1, 3)], \quad (117)$$

$$B = 2x_T s [D_0(1, 2, 3) + D_0(2, 1, 3) + D_0(1, 3, 2)]. \quad (118)$$

Finally, the A_{24} and A_{25} amplitudes read

$$A_{24} = (4\mathcal{G}_{\phi_a WW}\mathcal{G}_{\phi_b WW})\left(\frac{s}{x_T}\right)\left\{(x_t^2 + x_u^2 + 2x_a x_b)C_0(1, 2) - (x_t^2 + x_u^2 - 2x_a x_b)(x_t + x_u)C_0(3, 4) - (x_t^2 + x_a x_b)\left[(x_a - x_t)C_0(2, 3) + (x_b - x_t)C_0(1, 4)\right] - (x_u^2 + x_a x_b)\left[(x_a - x_u)C_0(1, 3) + (x_b - x_u)C_0(2, 4)\right] + s\left(x_T\left[-2x_W(x_t + x_u) + x_T\right]D_0(1, 3, 2) + \left[-2x_W x_T(x_u + x_t) + x_T^2 - x_t(x_a x_b + x_t^2)\right]D_0(1, 2, 3) + \left[-2x_W x_T(x_u + x_t) + x_T^2 - x_u(x_a x_b + x_u^2)\right]D_0(2, 1, 3)\right)\right\}, \quad (119)$$

$$A_{25} = \left(\mathcal{G}_{W^\pm H^\mp \phi_a}\mathcal{G}_{W^\pm H^\mp \phi_b}\right)\left(\frac{s}{x_T}\right)\left[\sum_{a=1}^{12} f_a^2 C_0(a) + s \sum_{a=1}^6 g_a^2 D_0(a)\right], \quad (120)$$

where

$$f_1^2 = f_2^2 = (f + 2)[(x_t - x_u)^2 + 2x_T] \quad (121)$$

$$f_3^2 = -(f + 2)(2x_H - 2x_W + x_u + x_t), \quad (122)$$

$$f_4^2 = (f + 2)(2x_H - 2x_W - x_u - x_t) - 8x_T \quad (123)$$

$$f_5^2 = f_6^2 = (x_a - x_u)[fx_u - 2(x_a - x_u)(x_b - x_u)], \quad (124)$$

$$f_7^2 = f_8^2 = (x_a - x_t)[fx_t - 2(x_a - x_t)(x_b - x_t)], \quad (125)$$

$$f_9^2 = f_{10}^2 = (x_b - x_t)[fx_t - 2(x_a - x_t)(x_b - x_t)], \quad (126)$$

$$f_{11}^2 = f_{12}^2 = (x_b - x_u)[fx_u - 2(x_a - x_u)(x_b - x_u)], \quad (127)$$

On the other hand,

$$g_1^2 = (f + 2)[2x_T x_H + (x_H - x_W + x_u)^2], \quad (128)$$

$$g_2^2 = \frac{1}{4}\left\{(f + 2)(2x_H - 2x_W + x_t + x_u)^2 - 2[4x_T + (f + 2)(x_t + 3x_u)](2x_H - 2x_W + x_t + x_u) + f[8x_T x_W + (x_t + 3x_u)^2] + 2[8x_T^2 + 4(2x_W + x_t + 3x_u)x_T + (x_t + 3x_u)^2]\right\}, \quad (129)$$

$$g_3^2 = (f + 2)[2x_T x_H + (x_H - x_W + x_t)^2], \quad (130)$$

$$g_4^2 = \frac{1}{4}\left\{(f + 2)(2x_H - 2x_W + x_t + x_u)^2 - 2[4x_T + (f + 2)(x_u + 3x_t)](2x_H - 2x_W + x_t + x_u) + f[8x_T x_W + (x_u + 3x_t)^2] + 2[8x_T^2 + 4(2x_W + x_u + 3x_t)x_T + (x_u + 3x_t)^2]\right\}, \quad (131)$$

$$g_5^2 = g_6^2 = \frac{1}{4}\left\{(f + 2)(2x_H - 2x_W + x_t + x_u)^2 + 2[f(x_T - x_t - x_u) - 2(x_t + x_u)](2x_H - 2x_W + x_t + x_u) + 8x_T x_W(f + 2) + 8x_T^2 - 2f(x_t + x_u)x_T + (f + 2)(x_t + x_u)^2\right\}. \quad (132)$$

C. The process $\gamma\gamma \rightarrow A\phi_a$

Bosonic loops do not contribute to this process. The fermionic contributions are given through diagrams of the type (i) in Figs. 1 and 3. The corresponding amplitudes can be written as follows:

$$\tilde{A}_1 = \tilde{F}_{11} + \tilde{F}_{13}, \quad (133)$$

$$\tilde{A}_2 = \tilde{F}_{23}, \quad (134)$$

where, the subscript j in \tilde{F}_{ij} stands for the contribution of the particular set of diagrams. Using the same notation defined above, the partial amplitudes read

$$\tilde{F}_{11} = \tilde{F}_{11}^A + \tilde{F}_{11}^Z, \quad (135)$$

where \tilde{F}_{11}^A (\tilde{F}_{11}^Z) represents the contribution due to Higgs boson A (Z boson). We can write these factors as

$$\tilde{F}_{11}^A = - \sum_f N_f Q_f^2 \left(\mathcal{G}_{A\bar{f}f} \mathcal{G}_{\phi_a AA} \right) \frac{x_f}{1 - x_A + i\sqrt{x_A} \gamma_A} s C_0(1, 2), \quad (136)$$

$$\tilde{F}_{11}^Z = \frac{1}{32\pi^3 c_W^2} \frac{x_u - x_t}{1 - x_Z + i\sqrt{x_Z} \gamma_Z} \mathcal{G}_{ZA\phi_a} \sum_f g_A^f Q_f^2 \int_0^1 dx_1 \int_0^{1-x_1} dx_2 \frac{x_1 x_2}{x_f - x_1 x_2}. \quad (137)$$

The expression given in Eq.(137) corresponds to the one given in Ref. [67].

$$\begin{aligned} \tilde{F}_{13} = & \sum_f N_f Q_f^2 \left(\mathcal{G}_{A\bar{f}f} \mathcal{G}_{\phi_a \bar{f}f} \right) \left(\frac{x_f}{x_W} \right) s \left\{ x_T (x_A - x_a) s D_0(1, 3, 2) + \right. \\ & 2x_f (1 + x_A - x_a) s \left[D_0(1, 2, 3) + D_0(2, 1, 3) + D_0(1, 3, 2) \right] + \\ & \left. (x_a - x_A) \left[(x_t - x_a) C_0(2, 3) + (x_t - x_A) C_0(1, 4) + (x_u - x_a) C_0(1, 3) + (x_u - x_A) C_0(2, 4) \right] \right\}, \end{aligned} \quad (138)$$

$$\begin{aligned} \tilde{F}_{23} = & \sum_f N_f Q_f^2 \left(\mathcal{G}_{A\bar{f}f} \mathcal{G}_{\phi_a \bar{f}f} \right) \left(\frac{x_f}{x_W} \right) s \left\{ s \left[x_t \left(\frac{x_a x_A - x_t^2}{x_T} \right) D_0(1, 2, 3) - x_u \left(\frac{x_a x_A - x_u^2}{x_T} \right) D_0(2, 1, 3) \right] + \right. \\ & 2x_f (x_u - x_t) s \left[D_0(1, 2, 3) + D_0(2, 1, 3) + D_0(1, 3, 2) \right] + \\ & \left(\frac{x_a x_A - x_u^2}{x_T} \right) \left[(x_u - x_a) C_0(1, 3) + (x_u - x_A) C_0(2, 4) \right] - \\ & \left(\frac{x_a x_A - x_t^2}{x_T} \right) \left[(x_t - x_a) C_0(2, 3) + (x_t - x_A) C_0(1, 4) \right] - \\ & \left. (x_u - x_t) \left[\left(\frac{x_t + x_u}{x_T} \right) C_0(1, 2) + \left(\frac{4x_a x_A - (x_t + x_u)^2}{x_T} \right) C_0(3, 4) \right] \right\}. \end{aligned} \quad (139)$$

V. NUMERICAL RESULTS AND DISCUSSION

We now turn to discuss our results. We refer to our three benchmark scenarios already discussed, namely, (1) Scenario I (the decoupling limit), (2) Scenario II (SM-like), and (3) Scenario III (a more general case of 2HDM-III).

A. Scenario I (the decoupling limit)

The main purposes of this subsection is to show explicitly how the decoupling of the charged Higgs effects operate according the criteria established in Ref. [50]. In this scenario, one assumes the existence of a light Higgs boson h , with mass of order of the Fermi scale v , whereas the rest of Higgs bosons are assumed very heavy, *i.e.*, $m_{H^\pm} \sim m_A \sim m_H \gg v$. The heavy Higgs boson effects decouple through two essentially different mechanisms [50], namely, by assuming $\mu_{12}^2 \gg v^2$ or $\mu_{12}^2 \sim v^2$ but taking large $\tan\beta$ or $\cot\beta$, depending on the configuration chosen for the λ_6 and λ_7 parameters. Accordingly, we will consider the following two cases:

Case A $m_h = 120 \text{ GeV}$, $\alpha = \beta - \pi/2$, $\lambda_6 = \lambda_7 = 0$, $\mu_{12}^2 \gg v^2$, and $m_H^+ \gg m_h$.

Case B $m_h = 120 \text{ GeV}$, $\alpha = \beta - \pi/2$, $\lambda_6 = -\lambda_7 = 0.1$, $\mu_{12}^2 \sim v^2$, and $m_H^+ \gg m_h$.

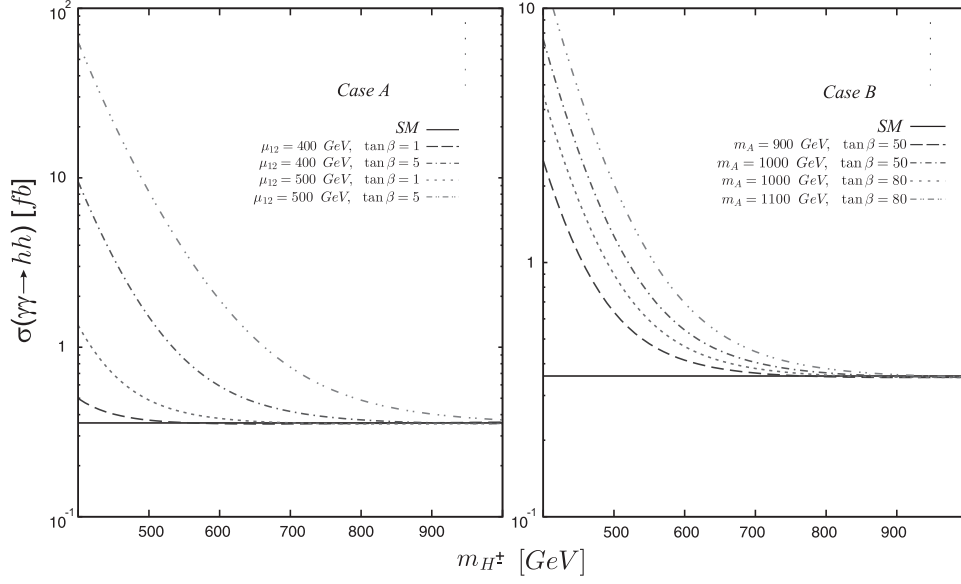


FIG. 6: Behavior of cross section for the process $\gamma\gamma \rightarrow hh$ as a function of the charged Higgs mass in the Scenario I (decoupling limit). The diverse values of the parameters as well as the case in consideration (A or B) are shown in the figure. In all cases the center-of-mass energy $\sqrt{s} = 500 \text{ GeV}$ was used.

In the Figure 6, we present the cross section of the process $\sigma(\gamma\gamma \rightarrow hh)$ as a function of the charged Higgs mass m_{H^\pm} . One can get the SM result (represented in these figures by the horizontal thick line) when $m_{H^\pm} \gg m_h$, showing the decoupling nature of this contribution. On the other hand, we can see from Fig. 7 that in the limit $\tan\beta \ll 1$ of the case A the SM result is obtained. The decoupling nature of the contributions for the case B is clearly appreciated when $\tan\beta \gg 1$.

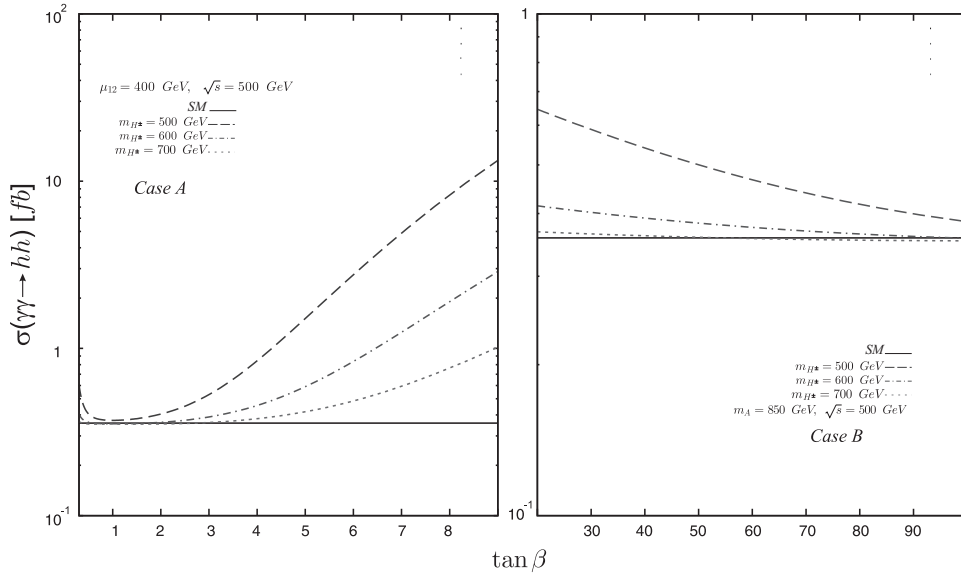


FIG. 7: Behavior of the cross section for the process $\gamma\gamma \rightarrow hh$ as a function of $\tan\beta$ in the Scenario I (decoupling limit). The diverse values of the parameters as well as the case in consideration (A or B) are shown in the figure. In all cases the center-of-mass energy $\sqrt{s} = 500 \text{ GeV}$ was used.

B. Scenario II (SM-like)

As already commented, in this scenario the couplings hVV ($V = W, Z$), hhh , $hhhh$ are nearly indistinguishable from the corresponding ones of the SM, but the hff couplings can deviate significantly from their SM counterparts $h_{SM}f\bar{f}$. In this context, we will use the values $m_h = 120$ GeV, $m_A = 110$ GeV, $m_H = m_{H^\pm} = m_A + m_h$, and $\mu_{12} = 130$ GeV in the two cases ($\lambda_6 = -\lambda_7 = 0.1$) and ($\lambda_6 = -\lambda_7 = 1$). The values $\chi_{uu,dd} = 1, -1$, which arise from a selection of a specific texture of the Yukawa matrices, will be used. In addition, we will assume that $\alpha = \beta \pm \pi/2$.

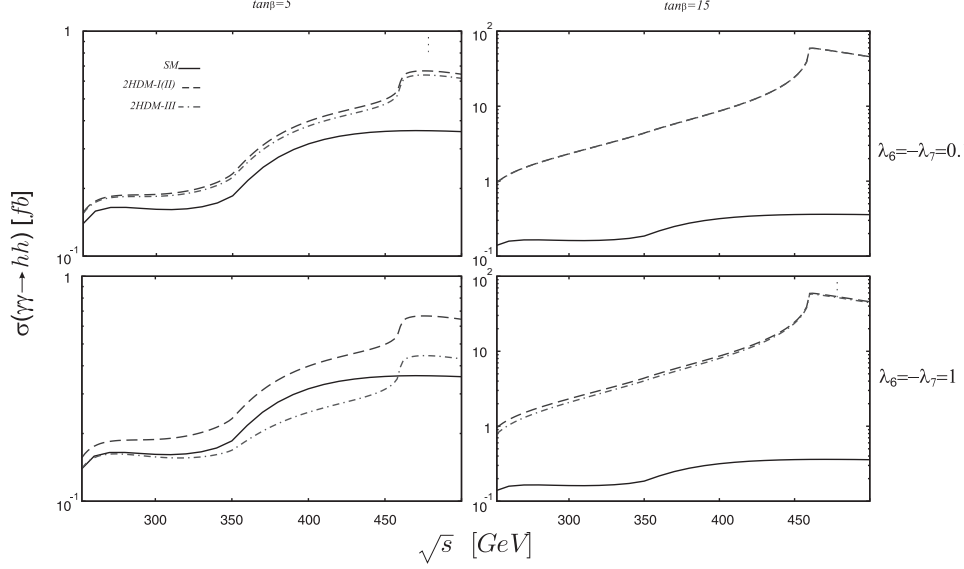


FIG. 8: Behavior of cross section for the process $\gamma\gamma \rightarrow hh$ as a function of center-of-mass energy \sqrt{s} in the Scenario II (SM-like). The curves correspond to SM (solid line), 2HDM type I-II (dashed line), and 2HDM-III (dashed-dotted line), for $\tan\beta = 5$ (left), 15 (right) in the case $\lambda_6 = -\lambda_7 = 0.1$ (up panels), 1 (down panels).

In Fig. 8, the cross section for the process $\gamma\gamma \rightarrow hh$ as a function of center-of-mass energy \sqrt{s} is shown. It can be appreciated that for $\tan\beta = 5$ both the SM and the 2HDM's predictions essentially coincide. However, one can see that for $\tan\beta = 15$ the cross section predicted by the 2HDMs could be two order of magnitude larger than the SM result. The results for $\chi = 1, -1$ are very similar. In this case, the cross section of the mode $\sigma(\gamma\gamma \rightarrow hh) \sim 70$ fb.

On the other hand, in Fig. 9, the cross sections for the $\gamma\gamma \rightarrow AA$ reaction as a function of the center-of-mass energy \sqrt{s} is displayed and the predictions of the 2HDM-III compared with those generated by the 2HDM-II. In this process we also consider the contribution of the parameters of the Higgs potential ($\lambda_6 = -\lambda_7 = 0.1$) (up panels) and ($\lambda_6 = -\lambda_7 = 1$) (down panels). We can observe that the main impact for the cross section comes from ($\lambda_6 = -\lambda_7 = 1$) and $\tan\beta$ large. The cross section of this mode could be enhanced by two orders of magnitude compared with the case $\lambda_6 = -\lambda_7 = 0.1$ or the usual case $\lambda_6 = -\lambda_7 = 0$ (2HDM-II). One can get $\sigma(\gamma\gamma \rightarrow AA) \sim 5 \times 10^5$ fb for $\tan\beta = 15$, with $\sqrt{s} = 450$ GeV, taking $\chi = 1, -1$ and $\lambda_6 = -\lambda_7 = 1$. The results for the cross section of the process $\gamma\gamma \rightarrow HH$ are shown in Fig. 10 for the same parameters of the previous process. Likewise, the cross section predicted by the 2HDM-III is two orders of magnitude larger than the one predicted by the 2HDM-II. We can obtain $\sigma(\gamma\gamma \rightarrow HH) \sim 1 \times 10^6$ fb for $\tan\beta = 15$, $\chi = 1, -1$, with $\sqrt{s} = 500$ GeV and $\lambda_6 = -\lambda_7 = 1$. As far as the cross section for the $\sigma(\gamma\gamma \rightarrow hH)$ process is concerned, its behavior as a function of the center-mass energy \sqrt{s} is shown in Fig. 11. From this figure, a considerable enhancement of the cross section compared with the 2HDM-II prediction can be observed for $\lambda_6 = 1 = -\lambda_7$. In this case, $\sigma(\gamma\gamma \rightarrow hH) \sim 5 \times 10^4$ fb for $\tan\beta = 15$, around $\sqrt{s} = 470$ GeV and $\chi = 1, -1$. It is worth commenting that this is the first time that this process is studied. Another process which has not been studied in the literature is $\sigma(\gamma\gamma \rightarrow hA)$. The corresponding cross sections as a function of the center-mass energy \sqrt{s} is shown in Fig. 12. It can be appreciated from this figure the importance of the cross section for the case $\lambda_6 = 1 = -\lambda_7$ and $\tan\beta = 15$, which is quite large as compared with the prediction of 2HDM-II where the λ_6 and λ_7 parameters are absent. It can be appreciated that the cross section could be of the order of 7 fb for $\sqrt{s} = 350$ GeV. On the other hand, when $\lambda_6 = -\lambda_7 \ll 1$ the cross section is very insignificant to be considered as relevant signals of neutral Higgs bosons. The last numerical results of this scenario is the cross section for the process $\gamma\gamma \rightarrow HA$, which is shown as a function of the center-mass energy in Fig. 13. It can be appreciated an important value for the cross section of about 2×10^3 fb for the case $\lambda_6 = -\lambda_7 = 1$, $\chi = -1$, $\tan\beta = 15$, and \sqrt{s} around 350 GeV.

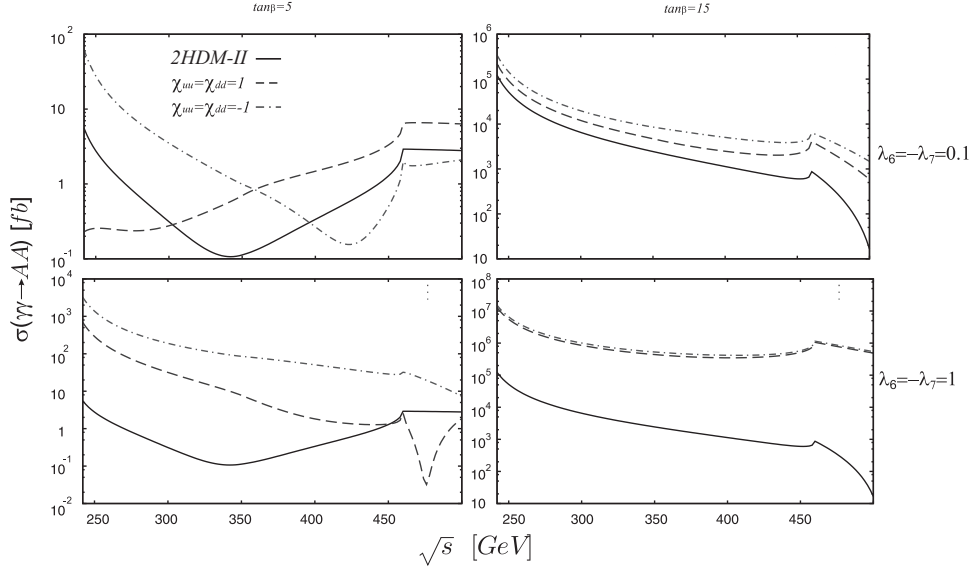


FIG. 9: Behavior of the cross section for the process $\gamma\gamma \rightarrow AA$ as a function of the center-of-mass energy \sqrt{s} in the Scenario II (SM-like). The lines correspond to 2HDM-II (solid line), 2HDM-III with $\chi_{uu,dd} = 1$ (dashed line) and 2HDM-III when $\chi_{uu,dd} = -1$ (dashed-dotted line), for $\tan\beta = 5$ (left), 15 (right) in the cases $\lambda_6 = -\lambda_7 = 0.1$ (up panels) and $\lambda_6 = -\lambda_7 = 1$ (down panels).

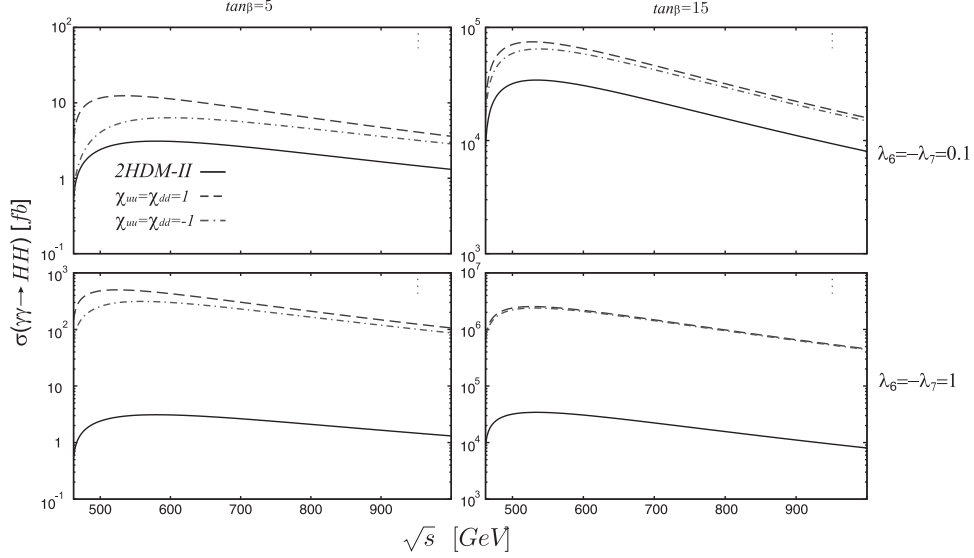


FIG. 10: Behavior of the cross section for the process $\gamma\gamma \rightarrow HH$ as a function of the center-of-mass energy \sqrt{s} in the Scenario II (SM-like). The description of the plots is the same as in Fig. 9.

C. Scenario III (a more general case of 2HDM-III)

As already commented, this scenario is much more general than the scenario II, because arbitrary couplings of neutral Higgs bosons to SM particles are assumed. Also, the contributions of the Higgs potential λ_6 and λ_7 parameters, as well as the contributions of the Yukawa texture in the couplings $\phi f \bar{f}$, are included. As commented at the end of Sec. II, the degenerate and the nondegenerate cases, as well as the case with a light CP-odd scalar will be considered.

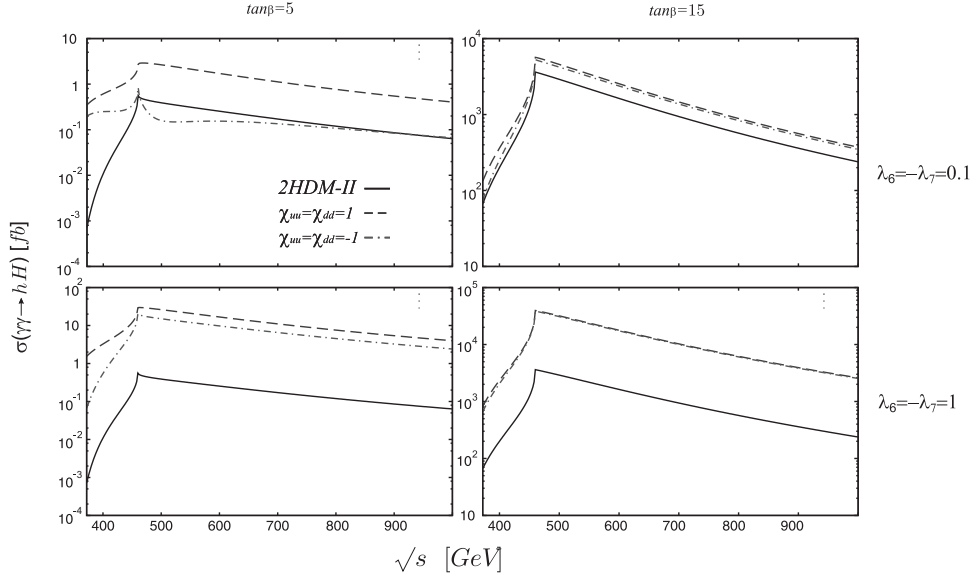


FIG. 11: Behavior of the cross section for the process $\gamma\gamma \rightarrow hH$ as a function of the center-of-mass energy \sqrt{s} in the Scenario II (SM-like). The description of the plots is the same as in Fig. 9.

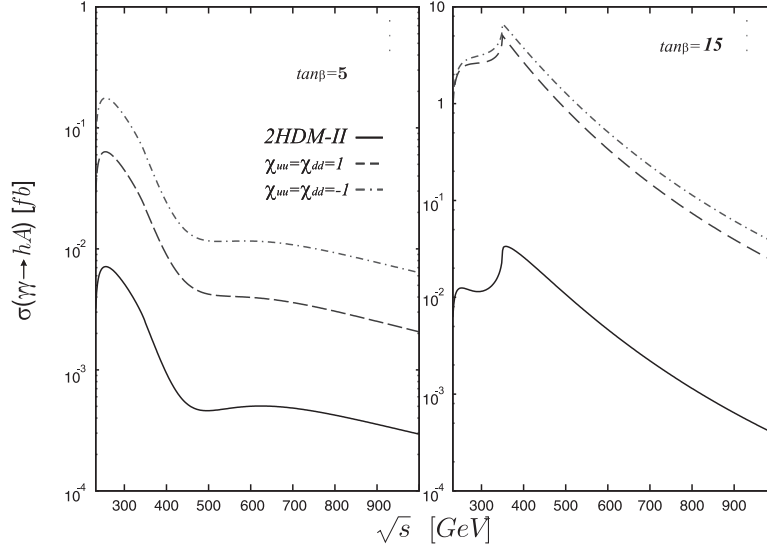


FIG. 12: Behavior of the cross section for the process $\gamma\gamma \rightarrow hA$ as a function of the center-of-mass energy \sqrt{s} in the Scenario II (SM-like). The lines correspond to 2HDM-II (solid line), 2HDM-III with $\chi_{uu,dd} = 1$ (dashed line) and 2HDM-III when $\chi_{uu,dd} = -1$ (dashed-dotted line), for $\tan\beta = 5$ (left), 15 (right) in the case $\lambda_6 = -\lambda_7 = 1$.

1. The nondegenerate case

We first discuss the nondegenerate case, defined by the values $m_{H^\pm} = 400$ GeV, $m_A = 350$ GeV, $M_H = 520$ GeV, $\mu_{12} = 120$ GeV, and $m_h = 120$ GeV. The set of values $\lambda_7 = -\lambda_6 = -1$ and $\lambda_7 = -\lambda_6 = -0.1$ are considered. In addition, it is assumed that $\alpha = \beta$ and $\alpha = \beta \pm \pi/2$.

In the down panels of Fig. 14, we show the cross section for the process $\gamma\gamma \rightarrow hh$ as a function of the center-of-mass energy \sqrt{s} . An important difference can be appreciated between two specific values of the Yukawa matrices with textures $\chi = 1$ and $\chi = -1$. For $\tan\beta = 5$ and $\chi = -1$, the cross section could be up to one order of magnitude larger than for the case $\chi = 1$, when $\sqrt{s} < 350$ GeV. In this region, we can get $\sigma(\gamma\gamma \rightarrow hh) \sim 1 \times 10^2$ fb for \sqrt{s} around 370 GeV. The cross section predicted by the 2HDM-II is two (one) order of magnitude lower than the 2HDM-III prediction with $\chi = -1$ (1). It can be seen that for $\sqrt{s} > 500$ GeV and $\chi = 1$ and $\chi = -1$, the cross section is of the same order of magnitude. However, in the 2HDM-III the cross section could be larger than the result obtained

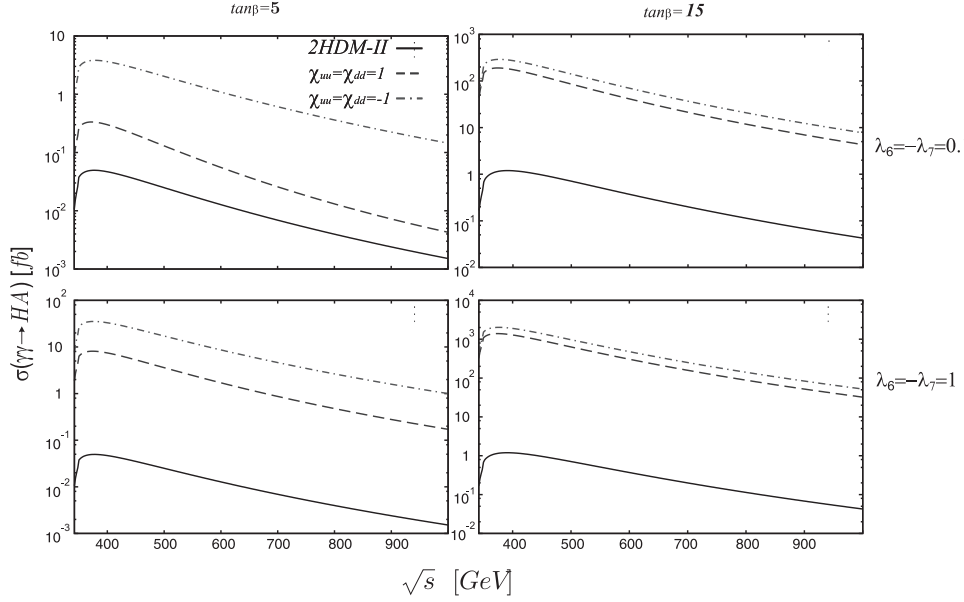


FIG. 13: Behavior of the cross section for the process $\gamma\gamma \rightarrow HA$ as a function of the center-of-mass energy \sqrt{s} in the Scenario II (SM-like). The description of the plots is the same as in Figure 9.

in the context of the 2HDM-II, due to the following choice $\lambda_6 = -\lambda_7 = 1$ of the parameters. In the same figure, it can be appreciated a spectacular enhancement of the cross section of $\sigma(\gamma\gamma \rightarrow hh) \sim 3 \times 10^7$ fb for $\tan\beta = 30$, $\chi = -1$, and $\sqrt{s} = 350$ GeV. The cross section predicted by the 2HDM-II is one order of magnitude lower than the one predicted by the 2HDM-III. On the other hand, it can be appreciated from the up panels of the same figure that in $\lambda_6 = -\lambda_7 = 0.1$ case, the corresponding cross sections are suppressed by about one order of magnitude with respect to those obtained in the $\lambda_6 = -\lambda_7 = 1$ case.

On the other hand, the cross section for the $\gamma\gamma \rightarrow HH$ reaction is shown in Fig. 15 as a function of the center-of-mass energy \sqrt{s} . The signal for this process could be relevant in the TeVs region, $\sqrt{s} > 1$ TeV. Therefore, this mode could be far away of the reach of early linear colliders. It can be appreciated from this figure that the predictions of the THDM-III approximates to that of the THDM-II in the case $\lambda_6 = -\lambda_7 = 0.1$.

As far as the $\gamma\gamma \rightarrow AA$ process is concerned, the corresponding cross section as a function of the center-of-mass energy \sqrt{s} is shown in Fig. 16. This mode is important in the 2HDM-III for center-of-mass energies above 700 GeV and for large values of $\tan\beta$. From this figure, it can be appreciated that in the case $\lambda_6 = -\lambda_7 = 1$ (up set of graphics in Fig. 16), $\sigma(\gamma\gamma \rightarrow AA) \sim 1 \times 10^6$ fb for $\sqrt{s} = 800$ GeV, $\tan\beta = 30$, and $\alpha = \beta$ or $\alpha = \beta \pm \pi/2$. The 2HDM-III predictions are two orders of magnitude larger than the ones of 2HDM-II. In the scenario with $\tan\beta = 5$, the cross section predicted by 2HDM-III is of order of 10 fb for $\sqrt{s} = 800$, $\chi = 1$, and $\alpha = \beta$, whereas the 2HDM-II prediction is about one order of magnitude lower. However, the situation changes drastically when $\alpha = \beta \pm \pi/2$, as in this case the 2HDM-II contribution dominates. On the other hand, it can be appreciated from these figures that in the case $\lambda_6 = -\lambda_7 = 0.1$ (down set of graphics in Fig. 16), the corresponding cross sections are of the same order of magnitude that those predicted by the THDM-II.

We now turn to discuss the process $\gamma\gamma \rightarrow hH$. The corresponding cross section as a function of the center-of-mass energy \sqrt{s} is shown in Fig. 17, in which the up set of graphics corresponds to the case $\lambda_6 = -\lambda_7 = 1$, whereas the down set was obtained using the values $\lambda_6 = -\lambda_7 = 0.1$. It is found that this process is sensitive to $\tan\beta$ and the mixing angle α . The cross section can reach a value of 20 fb for $\tan\beta = 5$ and $\alpha = \beta$. For large $\tan\beta$ values, the cross section is enhanced by several orders of magnitude. In fact, $\sigma(\gamma\gamma \rightarrow hH) \sim 1(5) \times 10^4$ fb for $\sqrt{s} = 800$ GeV, $\tan\beta = 30$, $\alpha = \beta$ ($\alpha = \beta \pm \pi/2$), and $\chi = \pm 1$. From these figures, it can be appreciated that the prediction of the THDM-III for the $\lambda_6 = -\lambda_7 = 0.1$ case is about one order of magnitude lower than that for the $\lambda_6 = -\lambda_7 = 1$ case, and clearly tends to the THDM-II prediction.

The cross section for the $\gamma\gamma \rightarrow hA$ as a function of the center-of-mass energy \sqrt{s} is shown in Fig. 18, in which the up set of graphics corresponds to the $\lambda_6 = -\lambda_7 = 1$ case, whereas the down set of figures arises from the $\lambda_6 = -\lambda_7 = 0.1$ case. This cross section is quite sensitive to the mixing angle α . A relevant value for the cross section arises when $\tan\beta$ is large and $\alpha = \beta$. In fact, $\sigma(\gamma\gamma \rightarrow hA) \sim 1 \times 10^4$ fb for $\sqrt{s} = 500$ GeV, $\tan\beta = 30$, and $\alpha = \beta$. It is important to notice that in the case $\lambda_6 = -\lambda_7 = 0.1$, only results for $\alpha = \beta$ are presented, as for $\alpha = \beta \pm \pi/2$ the cross sections are essentially independent on the λ_6 and λ_7 parameters, being therefore almost identical to those of the down panel

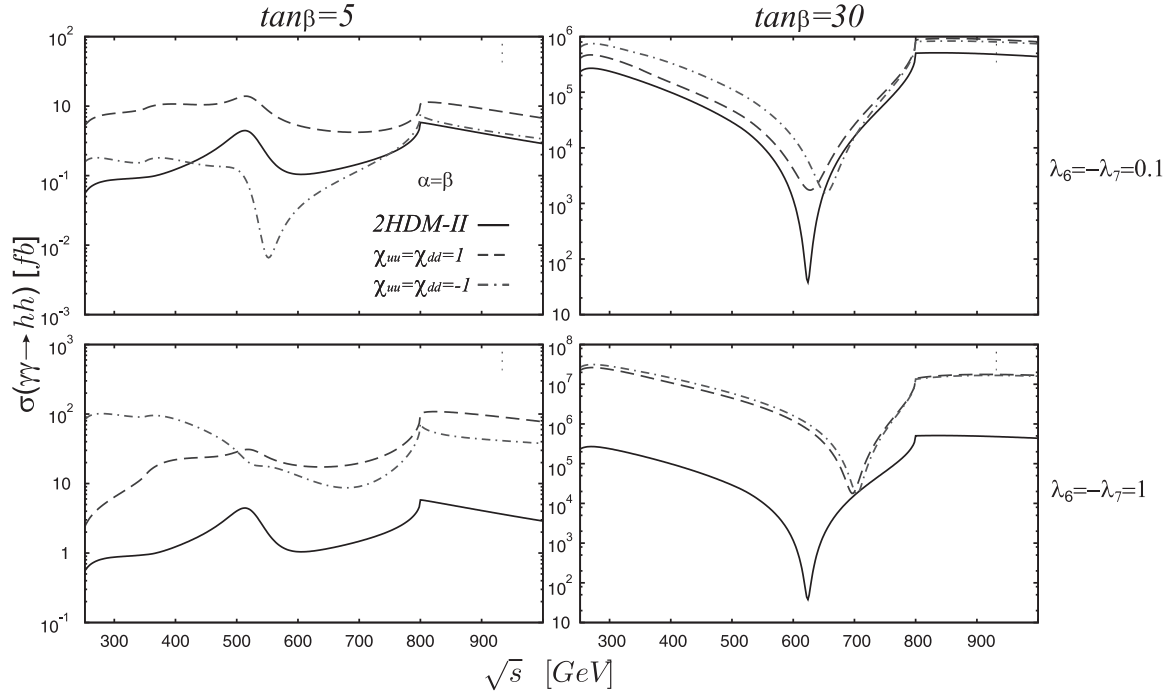


FIG. 14: Behavior of cross section for the process $\gamma\gamma \rightarrow hh$ as a function of the center-of-mass energy \sqrt{s} in the Scenario III (the nondegenerate case). The lines correspond to 2HDM-II (solid line), 2HDM-III with $\chi_{uu,dd} = 1$ (dashed line) and 2HDM-III when $\chi_{uu,dd} = -1$ (dashed-dotted line), for $\tan\beta = 5$ (left), 30 (right) in the cases $\lambda_6 = -\lambda_7 = 0.1$ (up panels) and $\lambda_6 = -\lambda_7 = 1$ (down panels). We choose the mixing angle $\alpha = \beta$.

of the up set of graphics. It can be appreciated from these figures that the cross sections for the $\lambda_6 = -\lambda_7 = 0.1$ case are about one order of magnitude lower than those for the $\lambda_6 = -\lambda_7 = 1$ case.

The cross section for the $\gamma\gamma \rightarrow HA$ process is shown in Fig. 19 as a function of the center-mass energy, in which the up set of graphics corresponds to the $\lambda_6 = -\lambda_7 = 1$ case, whereas the down set of figures arises from assuming $\lambda_6 = -\lambda_7 = 0.1$. Relevant cross sections are predicted by the 2HDM-III of order 10^2 fb for $\tan\beta = 30$, $\chi = \pm 1$, and energies around 900 GeV. It is important to notice that in the case $\lambda_6 = -\lambda_7 = 0.1$, only results for $\alpha = \beta + \pi/2$ are presented, as for $\alpha = \beta$ the cross sections are essentially independent on the λ_6 and λ_7 parameters, being therefore almost identical to those of the down panel of the up set of graphics. It can be appreciated from this figure that for $\tan\beta = 5$ the cross section in the $\lambda_6 = -\lambda_7 = 0.1$ case is one order of magnitude larger than in the $\lambda_6 = -\lambda_7 = 0.1$ case, in contrast with the behavior observed in all the other processes.

2. The degenerate case

In this paragraph, we present results for the degenerate case, which is defined in Sec. II. Only the case $\lambda_6 = -\lambda_7 = 1$ will be considered, as the $\lambda_6 = -\lambda_7 = 0.1$ case leads to cross sections suppressed by about one order of magnitude with respect to the former one. Although in general terms the cross sections for $\tan\beta = 30$ tend to be about two orders of magnitude larger than those obtained using $\tan\beta = 5$, we have preferred to make predictions using only the latter value because in this case the predictions of the two versions of the model (THDM-III and THDM-II) can be clearly distinguished.

In Fig. 20, the behavior of the cross sections for the processes $\gamma\gamma \rightarrow hh$ and $\gamma\gamma \rightarrow HH$ are shown as a function of the center-mass-energy, with $\alpha = \beta$ in the former process and $\alpha = \beta \pm \pi/2$ in the latter one. Besides to optimize the cross sections, this choice of values maximizes the differences between both models. It can be appreciated from this figures that the THDM-III predicts cross sections as large as 10^2 fb and 10 fb for the hh and HH channels, respectively, which are two and one orders of magnitude larger than those predicted by the THDM-II.

The cross sections for the processes $\gamma\gamma \rightarrow AA$ and $\gamma\gamma \rightarrow hH$ are shown in Fig. 21 as a functions of the center-mass-energy, for $\alpha = \beta$ in both cases. From this figure, it can be appreciated that the THDM-III prediction for the cross sections of both processes range from about 1 fb to 10 fb in the energies range shown. In contrast, the THDM-II predict cross sections quite suppressed (10^{-1} fb for $\gamma\gamma \rightarrow AA$ and 10^{-2} fb for $\gamma\gamma \rightarrow hH$), which varies slightly in all

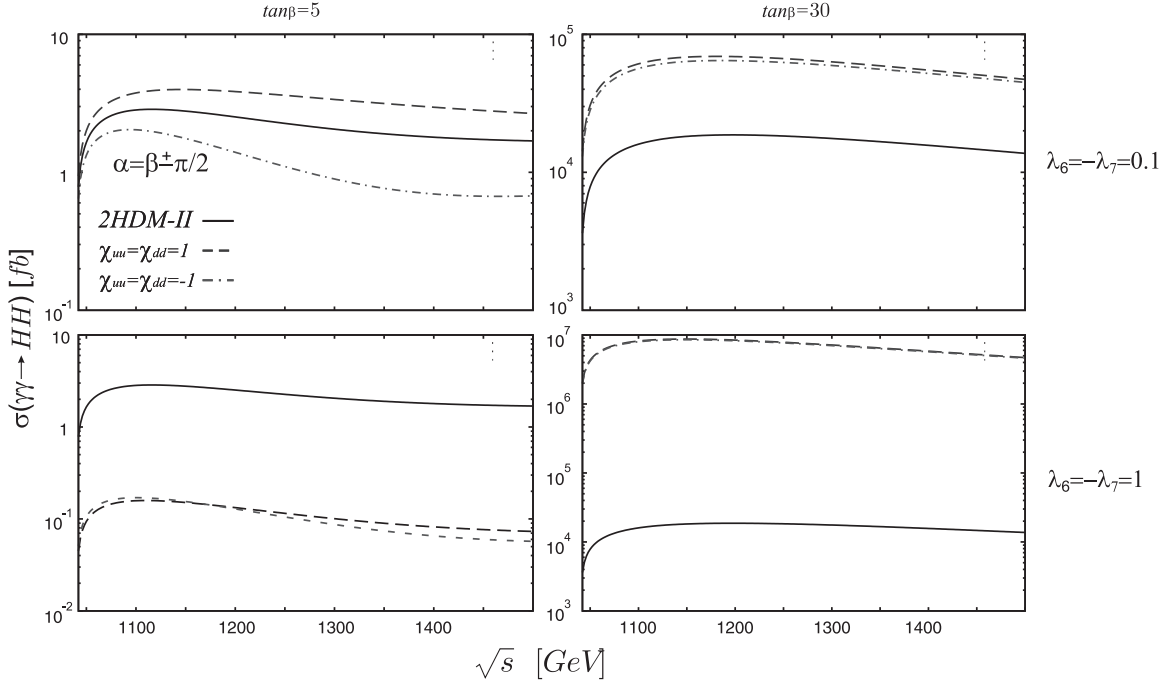


FIG. 15: Behavior of cross section for the process $\gamma\gamma \rightarrow HH$ as a function of the center-of-mass energy \sqrt{s} in the Scenario III, with a nondegenerate masses spectrum. The lines correspond to 2HDM-II (solid line), 2HDM-III with $\chi_{uu,dd} = 1$ (dashed line) and 2HDM-III when $\chi_{uu,dd} = -1$ (dashed-dotted line), for $\tan\beta = 5$ (left), 30 (right) in the cases $\lambda_6 = -\lambda_7 = 0.1$ (up panels) and $\lambda_6 = -\lambda_7 = 1$ (down panels). We choose the mixing angle $\alpha = \beta \pm \pi/2$.

the energies range considered.

The cross sections for the processes $\gamma\gamma \rightarrow hA$ and $\gamma\gamma \rightarrow HA$ are shown in Fig. 22 as a function of the center-mass-energy. The relations used between the α and β angles are shown in the figure. In this case, the predictions of the THDM-III ranges from 1 fb to 10 fb for the $\gamma\gamma \rightarrow hA$ process, whereas the prediction for the $\gamma\gamma \rightarrow HA$ reactions is one order of magnitude lower. The predictions of the THDM-II are quite suppressed, as both cross sections are of order of 10^{-2} fb or lower.

3. A light CP-odd scalar

In this paragraph, we discuss the very interesting case of a light CP-odd scalar A , which is allowed by the current constraints on the model. We consider the three possible processes, namely, $\gamma\gamma \rightarrow AA$, $\gamma\gamma \rightarrow HA$, and $\gamma\gamma \rightarrow hA$. In Fig. 23, the behavior of the cross sections for these processes as a functions of the center-mass-energy is shown, in a scenario with $m_A = 50\text{ GeV}$, $m_h = 120\text{ GeV}$, $m_{H^\pm} = 350\text{ GeV}$, $m_H = 400\text{ GeV}$, $\mu_{12} = 70\text{ GeV}$, and $\tan\beta = 5$. The value $\alpha = \beta \pm \pi/2$ for the $\gamma\gamma \rightarrow AA$ and $\gamma\gamma \rightarrow HA$ processes is assumed, whereas in the case of the $\gamma\gamma \rightarrow hA$ reaction it is assumed that $\alpha = \beta$. In all these processes, it is assumed that $\lambda_6 = -\lambda_7 = 1$ and that $\chi_{uu} = \chi_{dd} = \{1, -1\}$. Our notation and conventions are shown in the first graph of Fig. 23. From the first graph of this figure, it can be appreciated three resonant effects for the $\gamma\gamma \rightarrow AA$ process, centered at energies $\sqrt{s} = 120\text{ GeV} = m_h$, $\sqrt{s} = 400\text{ GeV} = m_H$, and $\sqrt{s} = 350\text{ GeV} = 2m_t$. The resonant effects due to m_h and m_H are spectacular, as the cross section can reach values of up to 10^8 fb and 10^6 fb , respectively. The resonant effect at $2m_t$ is less significative, as it occurs through a 1-loop fluctuation. Apart from these resonant effects, the values of the cross section are within the range of variation encountered in other scenarios analyzed previously, as the cross section predicted by the THDM-III ranges approximately from 10^{-1} fb to 1 fb in both the $\chi_{uu} = \chi_{dd} = -1$ and $\chi_{uu} = \chi_{dd} = 1$ scenarios, whereas in the THDM-II the corresponding cross section is about one order of magnitude larger. As far as the $\gamma\gamma \rightarrow HA$ process is concerned, it can be seen from this figure that the cross section predicted by the THDM-III ranges from 10^{-1} fb to 1 fb for the scenario with $\chi_{uu} = \chi_{dd} = -1$, whereas for $\chi_{uu} = \chi_{dd} = 1$ the cross section ranges from 10^{-3} fb to 10^{-2} fb . The corresponding cross section predicted by the THDM-II ranges from 10^{-2} fb to 10^{-1} fb in the same range of variation of the center-mass-energy. Finally, it can be appreciated from the third graph of Fig. 23 that the cross section for the $\gamma\gamma \rightarrow hA$ reaction ranges from 10 fb to 10^2 fb in the THDM-III in the scenario $\chi_{uu} = \chi_{dd} = -1$,

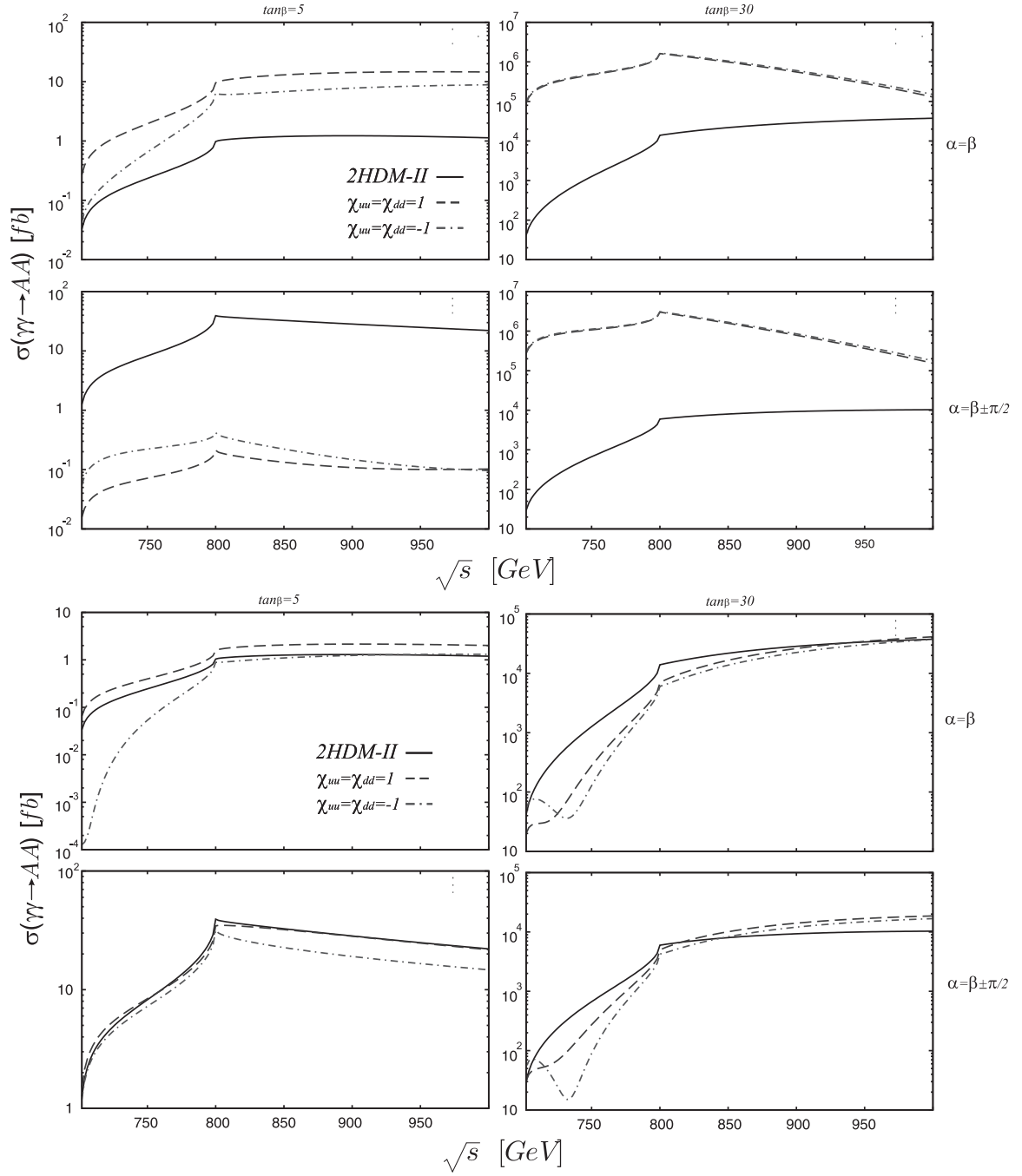


FIG. 16: Behavior of cross section for the process $\gamma\gamma \rightarrow AA$ as a function of the center-of-mass energy \sqrt{s} in the Scenario III, with a nondegenerate masses spectrum. The lines correspond to 2HDM-II (solid line), 2HDM-III with $\chi_{uu,dd} = 1$ (dashed line) and 2HDM-III when $\chi_{uu,dd} = -1$ (dashed-dotted line), for $\tan\beta = 5$ (left), 30 (right), taking $\alpha = \beta$ (up panels) and $\alpha = \beta \pm \pi/2$ (down panels). The up(down) set of graphics corresponds to the case $\lambda_6 = -\lambda_7 = 1$ ($\lambda_6 = -\lambda_7 = 0.1$).

and from 1 fb to 10 fb in the scenario $\chi_{uu} = \chi_{dd} = -1$. The corresponding cross section in the THDM-II is quite suppressed, as it ranges from 10^{-4} fb to 10^{-2} fb in the same domain of energies. The cross sections for all these processes can be enhanced by at least in one order of magnitude if $\tan\beta = 30$ is used instead of $\tan\beta = 5$.

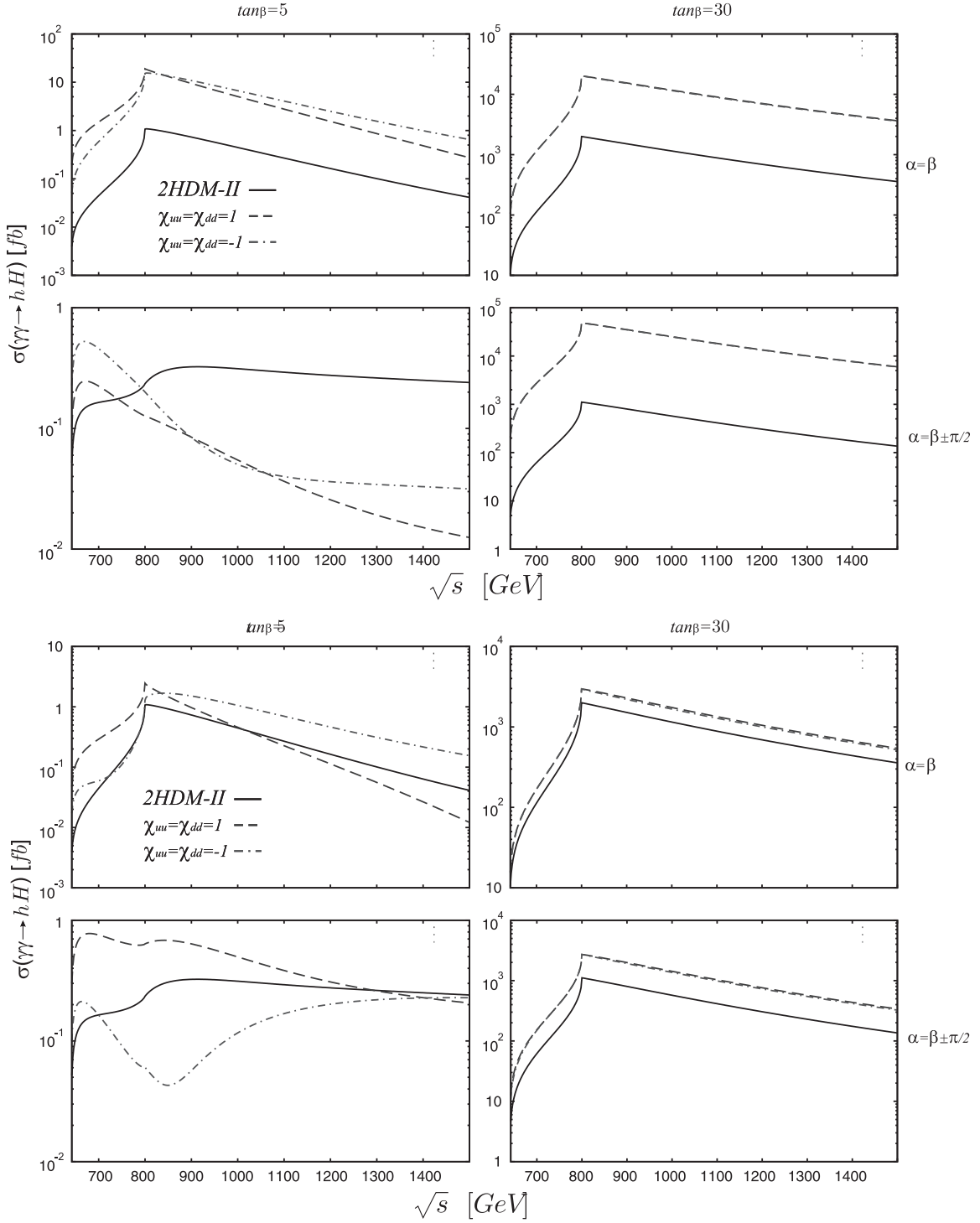


FIG. 17: The figure shows the behavior of cross section for the process $\gamma\gamma \rightarrow hH$ as a function of the center-of-mass energy \sqrt{s} in the Scenario III for the nondegenerate case. The description of the plots is the same as in Figure 16.

VI. SUMMARY

In this paper, a comprehensive study of the one-loop $\gamma\gamma \rightarrow \phi_i\phi_j$ ($\phi_i = h, H, A$) processes in the context of a general version of the two Higgs doublet model (2HDM-III) was presented. A nonlinear R_ξ -gauge, which allows us to define the W gauge boson propagator in a covariant way under the electromagnetic gauge group, was used. This gauge, which reduces significantly the number of Feynman diagrams to be considered in comparison with those that must

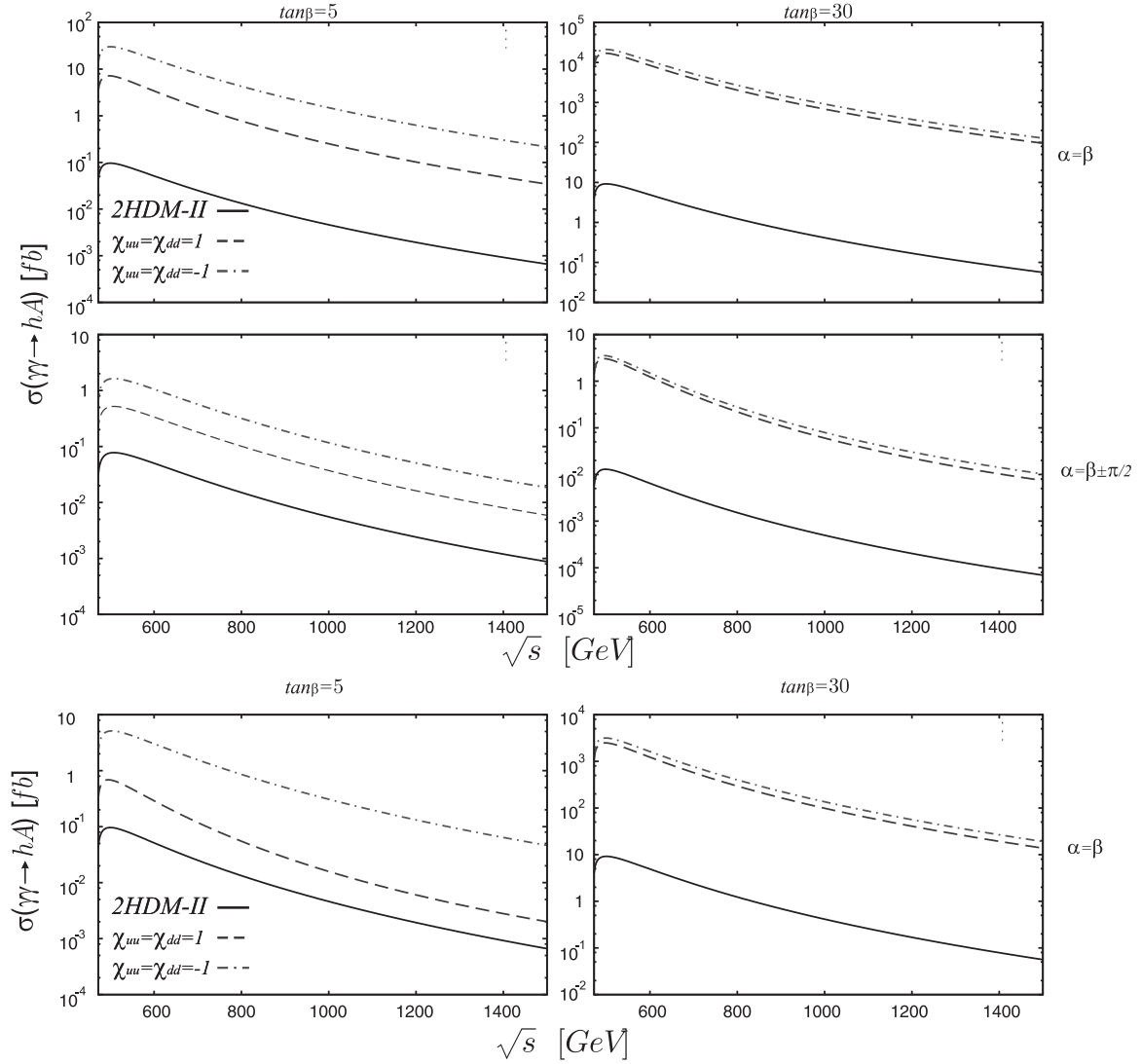


FIG. 18: The figure shows the behavior of cross section for the process $\gamma\gamma \rightarrow hA$ as a function of the center-of-mass energy \sqrt{s} in the Scenario III for the nondegenerate case. The description of the plots is the same as in Figure 16. In the down set of diagrams, only the case $\alpha = \beta$ is considered.

be calculated in conventional linear gauges, makes the issues of electromagnetic gauge invariance and cancelation of divergencies simpler. Explicit analytical expressions for all the possible modes, namely hh , HH , AA , hH , hA , and HA , were presented. The corresponding amplitudes are completely general in the sense that they can be used for any version of the 2HDM. The version of the 2HDM that is considered in this work, which we called simply 2HDM-III, comprise the implementation of a flavor symmetry in the Yukawa sector, namely a four-zero Yukawa Texture, which allows us to suppress FCNC effects without necessity of introducing a discrete symmetry. Due to this, a Higgs potential, more general than the one considered in the 2HDM-II version, can be introduced. This Higgs potential includes two dimensionless parameters, λ_6 and λ_7 , to which the cross sections for the $\gamma\gamma \rightarrow \phi_i\phi_j$ processes are quite sensitive. The $\gamma\gamma \rightarrow \phi_i\phi_j$ mechanisms for Higgs pair production were analyzed in three scenarios of the 2HDM-III. In the scenario I (the decoupling case), the $\gamma\gamma \rightarrow hh$ reaction was studied in the two possible cases in which the decoupling operates, namely, when $\mu_{12}^2 \gg v^2$ or $\mu_{12}^2 \sim v^2$ but assuming that $\tan\beta$ or $\cot\beta$ are large, depending on the configuration chosen for the λ_6 and λ_7 parameters. In both cases, it is found that, in the heavy mass limit of the charged Higgs, the cross section for this reaction approach to the well known SM result. In the scenario II (SM-like), it is assumed that the hVV ($V = W, Z$), hh , and $hhhh$ couplings are nearly indistinguishable from the corresponding ones of the SM, but the hff couplings can deviate significantly from their SM counterparts $h_{SM}f\bar{f}$. It was found that some combinations of Yukawa textures with the λ_6 and λ_7 parameters, together with large $\tan\beta$ lead to experimentally interesting cross sections. In the scenario III (a more general case of 2HDM-III), besides considering

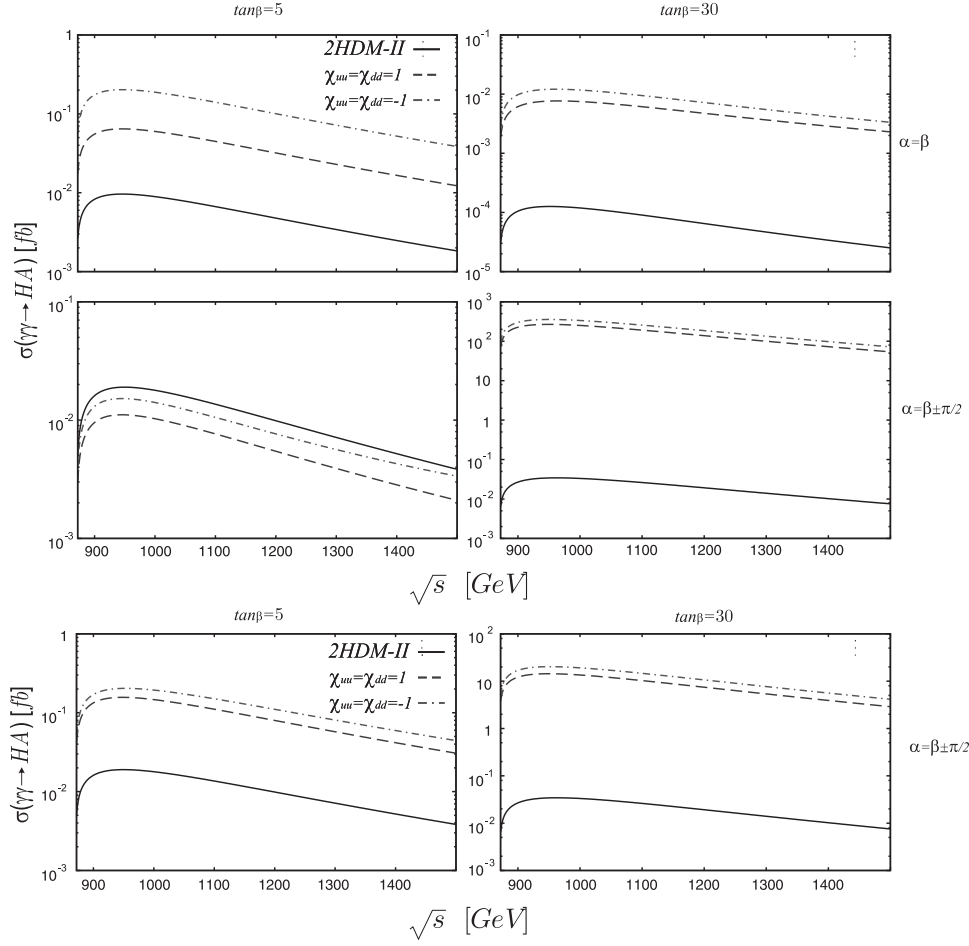


FIG. 19: Behavior of cross section for the process $\gamma\gamma \rightarrow HA$ as a function of the center-of-mass energy \sqrt{s} in the Scenario III for the nondegenerate case. The description of the plots is the same as in Figure 16. In the down set of diagrams, only the case $\alpha = \beta \pm \pi/2$ is considered.

the contributions of the Higgs potential through the λ_6 and λ_7 parameters, as well as the contributions of the Yukawa texture in the couplings $\phi f \bar{f}$, arbitrary couplings of neutral Higgs bosons to SM particles were assumed. In this scenario, the implications of a light CP-odd scalar was studied.

In general terms, we can conclude that the parameters of the Higgs potential λ_6 and λ_7 considerably enhance the cross sections for the $\gamma\gamma \rightarrow \phi_i \phi_j$ processes. In almost all cases, the results of 2HDM-III are two orders of magnitude larger than those obtained from the 2HDM-II. A considerable enhancement for the cross sections of the processes $\gamma\gamma \rightarrow \phi_i \phi_j$ was observed in the regime of large $\tan\beta$.

Appendix A: Feynman rules in the nonlinear gauge

We present the couplings for the most popular types of 2HDM (I, II, y III). The vertex can be written as

$$g_{\phi_i \bar{f} f} = -\frac{igm_f}{2m_W} \begin{cases} \mathcal{G}_{\phi_a \bar{f} f}, & \text{for } h, H \\ i\gamma^5 \mathcal{G}_{A \bar{f} f}, & \text{for } A \end{cases} \quad (\text{A1})$$

where $\mathcal{G}_{\phi_i \bar{f} f}$ are dimensionless functions expressed in the table (I).

1. Yang-Mills Couplings

This sector is strongly affected by the gauge-fixing procedure that we used. This couplings can be found in [44]. Here, we only present the Feynman rules associated with the vertices used in this work, namely, $A_\eta(k_1)W_\lambda^+(k_2)W_\rho^-(k_3)$

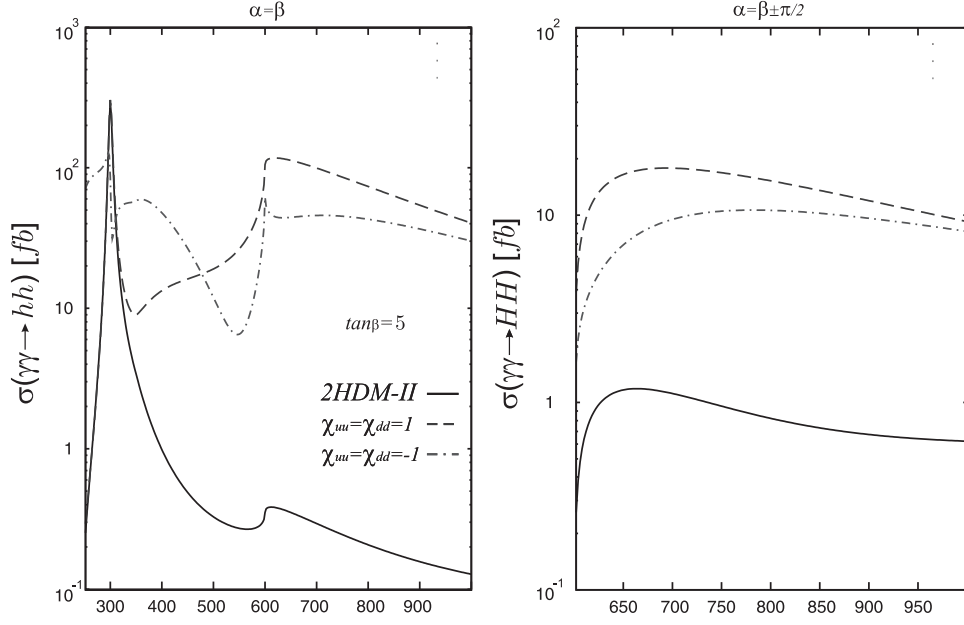


FIG. 20: Behavior of cross section for the processes $\gamma\gamma \rightarrow hh$ (left) and $\gamma\gamma \rightarrow HH$ (right) as a function of the center-of-mass energy \sqrt{s} in the Scenario III for the degenerate case.

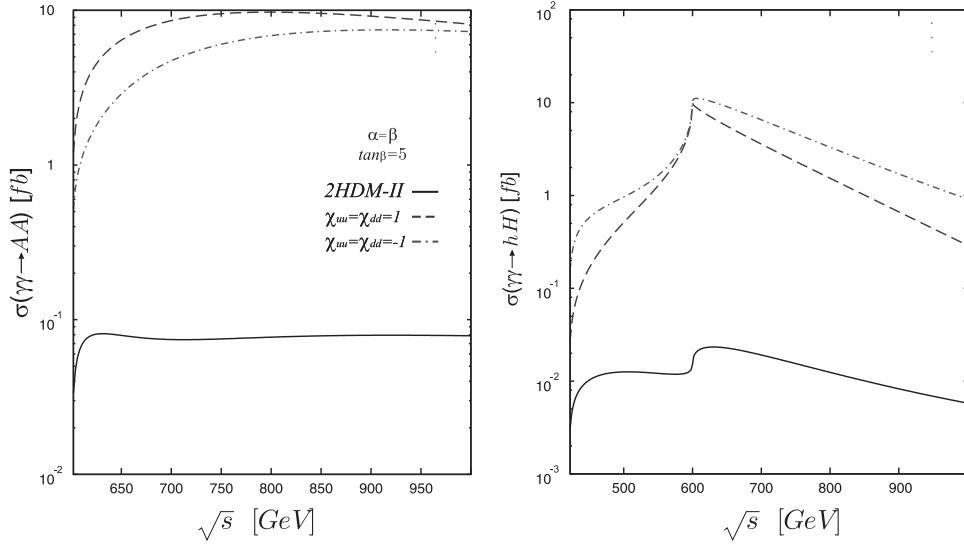


FIG. 21: Behavior of cross section for the processes $\gamma\gamma \rightarrow AA$ (left) and $\gamma\gamma \rightarrow hH$ (right) as a function of the center-of-mass energy \sqrt{s} in the Scenario III for the degenerate case.

and $A_\alpha A_\beta W_\lambda^+ W_\rho^-$. The corresponding vertex functions are given by

$$-ie\Gamma_{\lambda\rho\eta}(k_1, k_2, k_3) = -ie \left((k_3 - k_2)_\eta g_{\lambda\rho} + (k_1 - k_3 - \frac{1}{\xi}k_2)_\lambda g_{\rho\eta} + (k_2 - k_1 + \frac{1}{\xi}k_3)_\rho g_{\lambda\eta} \right), \quad (\text{A2})$$

$$-ie^2\Gamma_{\alpha\beta\lambda\rho} = -ie^2 \left(2g_{\alpha\beta}g_{\lambda\rho} - (1 - \frac{1}{\xi})(g_{\alpha\lambda}g_{\beta\rho} + g_{\alpha\rho}g_{\beta\lambda}) \right). \quad (\text{A3})$$

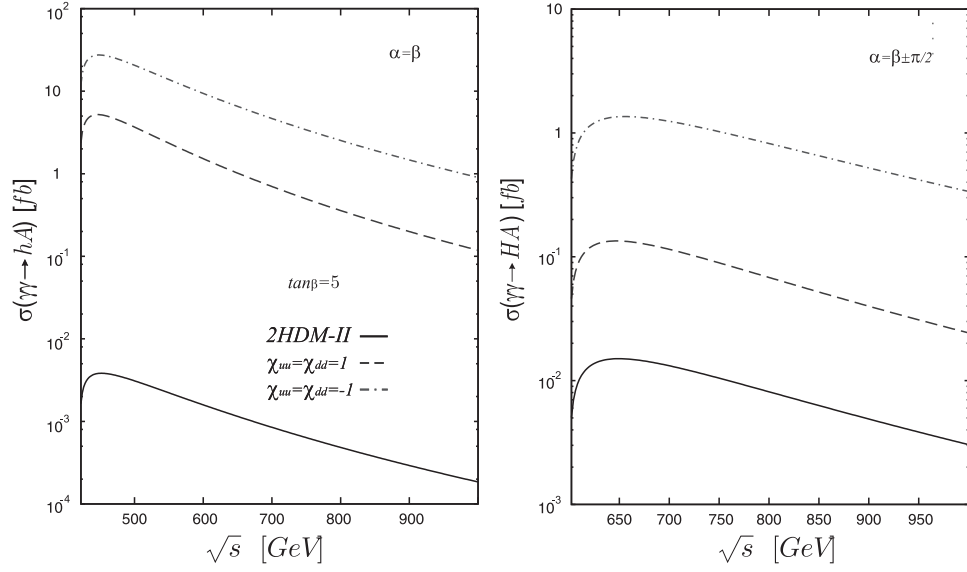


FIG. 22: Behavior of cross section for the processes $\gamma\gamma \rightarrow hA$ (left) and $\gamma\gamma \rightarrow HA$ (right) as a function of the center-of-mass energy \sqrt{s} in the Scenario III for the degenerate case.

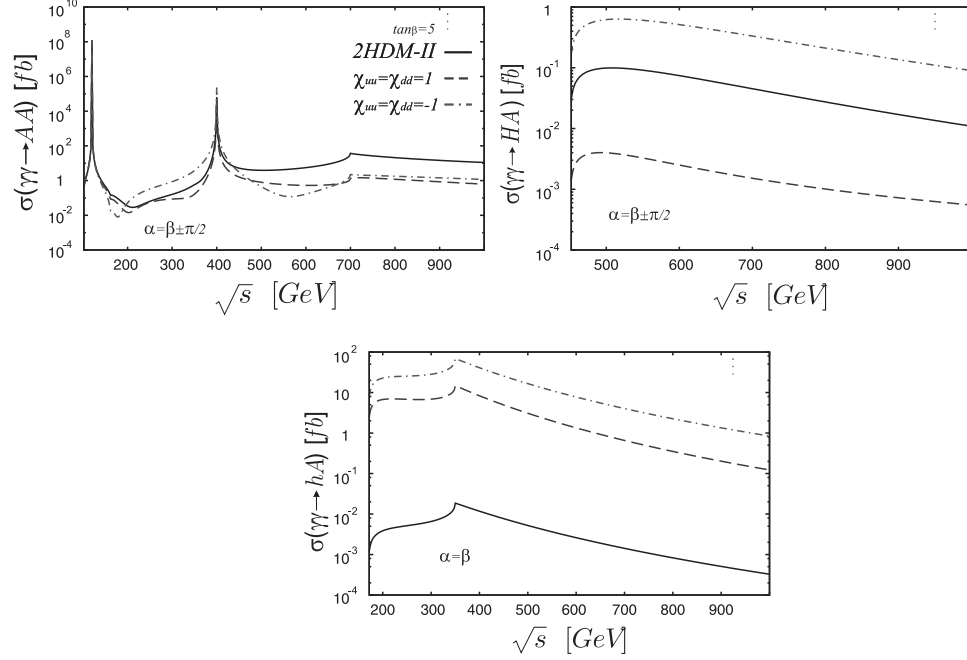


FIG. 23: Behavior of cross section for the processes $\gamma\gamma \rightarrow AA$, $\gamma\gamma \rightarrow HA$, and $\gamma\gamma \rightarrow hA$ as a function of the center-of-mass energy \sqrt{s} in the scenario of a light CP-odd scalar.

$\mathcal{G}_{\phi_i \bar{f} f}$	Type-I	Type-II	Type-III
$\mathcal{G}_{hll}, \mathcal{G}_{hdd}$	$\frac{c_\alpha}{s_\beta}$	$\frac{-s_\alpha}{c_\beta}$	$\frac{-s_\alpha}{c_\beta} + \frac{c_\alpha - \beta \chi_{dd}}{\sqrt{2}c_\beta}$
\mathcal{G}_{huu}	$\frac{c_\alpha}{s_\beta}$	$\frac{c_\alpha}{s_\beta}$	$\frac{c_\alpha}{s_\beta} - \frac{c_\alpha - \beta \chi_{uu}}{\sqrt{2}s_\beta}$
$\mathcal{G}_{Hll}, \mathcal{G}_{Hdd}$	$\frac{s_\alpha}{s_\beta}$	$\frac{c_\alpha}{c_\beta}$	$\frac{c_\alpha}{c_\beta} + \frac{s_\alpha - \beta \chi_{dd}}{\sqrt{2}c_\beta}$
\mathcal{G}_{Huu}	$\frac{s_\alpha}{s_\beta}$	$\frac{s_\alpha}{s_\beta}$	$\frac{s_\alpha}{s_\beta} - \frac{s_\alpha - \beta \chi_{uu}}{\sqrt{2}s_\beta}$
$\mathcal{G}_{A ll}, \mathcal{G}_{A dd}$	t_β^{-1}	$-t_\beta$	$-t_\beta + \frac{\chi_{dd}}{\sqrt{2}c_\beta}$
$\mathcal{G}_{A uu}$	$-t_\beta^{-1}$	$-t_\beta^{-1}$	$-t_\beta^{-1} + \frac{\chi_{uu}}{\sqrt{2}s_\beta}$

TABLE I: Dimensionless function that define the Yukawa couplings [12, 28, 30].

2. Scalar and Kinetic sector

Now we present the couplings that contain scalar particles, in particular the vertex functions necessary for our calculation. The vertex functions between scalar Higgs can be written as following:

$$g_{\phi_a \phi_b \phi_c} = \frac{-igm_W}{4} \mathcal{G}_{\phi_a \phi_b \phi_c}, \quad (\text{A4})$$

$$g_{\phi_i H^\pm H^\mp} = \frac{-igm_W}{4} \mathcal{G}_{\phi_i H^\pm H^\mp}, \quad (\text{A5})$$

$$g_{H^\pm H^\mp \phi_i \phi_j} = \frac{-ig^2}{16} \mathcal{G}_{H^\pm H^\mp \phi_i \phi_j} \quad (\text{A6})$$

$$g_{H^\pm G_W^\mp A} = \pm \frac{g(m_{H^\pm}^2 - m_A^2)}{2m_W} \quad (\text{A7})$$

$$g_{\phi_a AA} = \frac{-igm_W}{4} \mathcal{G}_{\phi_a AA} \quad (\text{A8})$$

The explicit form of this vertex function can be found in [50].

The couplings that involve a pair of W -Goldstone boson was modified by the gauge-fixing procedure. This couplings can be expressed as:

$$g_{G_W^\pm G_W^\mp \phi_i} = \frac{-ig(m_i^2 + 2\xi m_W^2)}{2m_W} \mathcal{G}_{\phi_i WW}, \quad (\text{A9})$$

$$g_{G_W^\pm G_W^\mp \phi_i \phi_j} = \frac{-ig^2}{16} \mathcal{G}_{G_W^\pm G_W^\mp \phi_i \phi_j}. \quad (\text{A10})$$

The explicit form of this couplings have to be take of the reference [44].

On the other hand, the couplings involving gauge and scalar fields are present in the table II. Here, the dimensionless functions \mathcal{G} can be written as:

$$\mathcal{G}_{hWW} = -\mathcal{G}_{W^\pm H^\mp H} = -\mathcal{G}_{ZAH} = s_{(\beta-\alpha)}, \quad (\text{A11})$$

$$\mathcal{G}_{HWW} = \mathcal{G}_{W^\pm H^\mp h} = \mathcal{G}_{ZAh} = c_{(\beta-\alpha)}. \quad (\text{A12})$$

Appendix B: The scalar functions

In this appendix we present the $C_0(a)$ and $D_0(a)$ scalar functions appearing in the amplitudes A_{15} and A_{25} associated with the processes $\gamma\gamma \rightarrow AA$ and $\gamma\gamma \rightarrow \phi_a \phi_b$.

TABLE II: Structure of the couplings involving gauge and scalar fields.

Coupling	Vertex Function	Coupling	Vertex Function
$g_{A_\mu H^-(p_-)H^+(p_+)}$	$ie(p_- - p_+)_\mu$	$g_{A_\mu A_\nu H^- H^+}$	$2ie^2 g_{\mu\nu}$
$g_{A_\mu G_W^-(p_-)G_W^+(p_+)}$	$ie(p_- - p_+)_\mu$	$g_{A_\mu A_\nu G_W^- G_W^+}$	$2ie^2 g_{\mu\nu}$
$g_{\phi_a W_\mu^- W_\nu^+}$	$igm_W \mathcal{G}_{\phi_a WW} g_{\mu\nu}$	$g_{(hh, HH, AA)W_\mu^- W_\nu^+}$	$\frac{ig^2}{2} g_{\mu\nu}$
$g_{\phi_a(p_a)W_\mu^\pm H^\mp(p_{H^\pm})}$	$\pm \frac{ig}{2} \mathcal{G}_{W^\pm H^\mp \phi_a}(p_{H^\pm} - p_a)_\mu$	$g_{A_\mu W_\nu^\pm H^\mp \phi_a}$	$\frac{ieg}{2} \mathcal{G}_{W^\pm H^\mp \phi_a} g_{\mu\nu}$
$g_{A(p_A)W_\mu^\pm H^\mp(p_{H^\pm})}$	$-\frac{g}{2}(p_{H^\pm} - p_A)_\mu$	$g_{A_\mu W_\nu^\pm H^\mp A}$	$\mp \frac{eg}{2} g_{\mu\nu}$
$g_{\phi_a(p)W_\mu^\pm G_W^\mp}$	$\mp igp_\mu \mathcal{G}_{\phi_a WW}$	$g_{ZA(p_A)\phi_a(p_a)}$	$\frac{g}{2c_W}(p_a - p_A)_\mu \mathcal{G}_{ZA\phi_a}$

$$C_0(1) = C_0(s, m_i^2, m_j^2, m_W^2, m_W^2, m_{H^\pm}^2), \quad (B1)$$

$$C_0(2) = C_0(s, m_i^2, m_j^2, m_{H^\pm}^2, m_{H^\pm}^2, m_W^2), \quad (B2)$$

$$C_0(3) = C_0(0, 0, s, m_{H^\pm}^2, m_{H^\pm}^2, m_{H^\pm}^2), \quad (B3)$$

$$C_0(4) = C_0(0, 0, s, m_W^2, m_W^2, m_W^2), \quad (B4)$$

$$C_0(5) = C_0(0, m_i^2, u, m_{H^\pm}^2, m_{H^\pm}^2, m_W^2), \quad (B5)$$

$$C_0(6) = C_0(0, m_i^2, u, m_W^2, m_W^2, m_{H^\pm}^2), \quad (B6)$$

$$C_0(7) = C_0(0, m_i^2, t, m_{H^\pm}^2, m_{H^\pm}^2, m_W^2), \quad (B7)$$

$$C_0(8) = C_0(0, m_i^2, t, m_W^2, m_W^2, m_{H^\pm}^2), \quad (B8)$$

$$C_0(9) = C_0(0, t, m_j^2, m_{H^\pm}^2, m_{H^\pm}^2, m_W^2), \quad (B9)$$

$$C_0(10) = C_0(0, t, m_j^2, m_W^2, m_W^2, m_{H^\pm}^2), \quad (B10)$$

$$C_0(11) = C_0(0, u, m_j^2, m_{H^\pm}^2, m_{H^\pm}^2, m_W^2), \quad (B11)$$

$$C_0(12) = C_0(0, u, m_j^2, m_W^2, m_W^2, m_{H^\pm}^2), \quad (B12)$$

$$D_0(1) = D_0(0, 0, m_i^2, m_j^2, s, u, m_{H^\pm}^2, m_{H^\pm}^2, m_{H^\pm}^2, m_W^2), \quad (B13)$$

$$D_0(2) = D_0(0, 0, m_i^2, m_j^2, s, u, m_W^2, m_W^2, m_W^2, m_{H^\pm}^2), \quad (B14)$$

$$D_0(3) = D_0(0, 0, m_i^2, m_j^2, s, t, m_{H^\pm}^2, m_{H^\pm}^2, m_{H^\pm}^2, m_W^2), \quad (B15)$$

$$D_0(4) = D_0(0, 0, m_i^2, m_j^2, s, t, m_W^2, m_W^2, m_W^2, m_{H^\pm}^2), \quad (B16)$$

$$D_0(5) = D_0(0, m_i^2, 0, m_j^2, u, t, m_{H^\pm}^2, m_{H^\pm}^2, m_W^2, m_W^2), \quad (B17)$$

$$D_0(6) = D_0(0, m_i^2, 0, m_j^2, u, t, m_W^2, m_W^2, m_{H^\pm}^2, m_{H^\pm}^2), \quad (B18)$$

where $m_i = m_j = m_A$ for $\gamma\gamma \rightarrow AA$, and $m_i = m_a$ and $m_j = m_b$ for $\gamma\gamma \rightarrow \phi_a \phi_b$.

Acknowledgments

We acknowledge support by Conacyt, SNI, and Red-FAE (Mexico). JH-S and CGH acknowledge R. Noriega-Papaqui for useful discussions.

-
- [1] See G. Aarons *et al.*, *ILC Global Designing Effort and World Wide Study*, arXiv:0712.1950V1 [physics.acc-ph], and references therein.
- [2] I. Ginzburg, G. Kotkin, V. Serbo, V. Telnov, *Pizma ZhETF*, **34**, 514 (1981); *JETP Lett.* **34**, 491 (1982); Preprint INP 81-50, 1981, Novosibirsk.; I. Ginzburg, G. Kotkin, V. Serbo, V. Telnov, *Nucl. Instr. Meth.* **205**, 47 (1983); I. Ginzburg, G. Kotkin, S. Panfil, V. Serbo, V. Telnov, *Nucl. Instr. Meth.* **219**, 5 (1984).
- [3] G. Tetlalmatzi, J. G. Contreras, F. Larios and M. A. Perez, *Phys. Rev. D* **81** (2010) 037303 [arXiv:0911.4472 [hep-ph]].

- [4] G. Aad *et al.* [ATLAS Collaboration], JINST **3**, S08003 (2008). ATLAS-CONF-2011-157
- [5] G. L. Bayatian *et al.* [CMS Collaboration], J. Phys. G **34**, 995 (2007). CMS-PAS-HIG-11-023
- [6] A. G. Akeroyd *et al.*, *Physics Interplay of the LHC and the ILC*, editors: G. Weiglein *et al.*, arXiv:hep-ph/0410364v1.
- [7] For a review see, E. Boos *et al.*, Nucl. Instrum. Meth. **A472**, 100 (2001), **hep-ph/0103090**.
- [8] I. F. Ginzburg, G. L. Kotkin, S. L. Panfil, V. G. Serbo, Nucl. Phys. **B228**, 285 (1983); Eran Yehudai, Phys. Rev. **D44**, 3434 (1991); J. P. Ma and B. H. J. McKellar, Phys. Lett. **B319**, 533 (1993); G. Belanger and G. Couture, Phys. Rev. **D49**, 5720 (1994); S. Y. Choi and K. Hagiwara, Phys. Rev. **D54**, 6703 (1996); M. Baillargeon, G. Bélanger, F. Boudjema, Nucl. Phys. **B500**, 224 (1997).
- [9] G. Bélanger and F. Boudjema, Phys. Lett. **B288**, 210 (1992); M. J. Herrero and E. Ruiz-Morales, Phys. Lett. **B296**, 397 (1992).
- [10] T. Barklow, *Proc. of the 1990 DPF Summer Study on Higs Energy Physics: Research Directions for the Decade*, Editor E. Berger, Snowmass, CO, 1990; J. F. Gunion and H. E. Haber, *ibid*; Phys. Rev. **D48**, 5109 (1993); D. L. Borden, D. A. Bauer, D. O. Caldwell, Phys. Rev. **D48**, 4018 (1993).
- [11] N. Bernal, D. Lopez-Val and J. Sola, Phys. Lett. B **677**, 39 (2009) [arXiv:0903.4978 [hep-ph]]. D. Lopez-Val and J. Sola, Phys. Lett. B **702**, 246 (2011) [arXiv:1106.3226 [hep-ph]]. J. Sola and D. Lopez-Val, arXiv:1107.1305 [hep-ph].
- [12] S. Dawson *et al.*, *The Higgs Hunter's Guide* (Addison-Wesley, New York, 1990).
- [13] Barger V D, Hewett J L and Phillips R J N 1990 Phys. Rev.D **41** 3421
- [14] A. G. Akeroyd, Phys. Lett. B **377**, 95 (1996) [hep-ph/9603445].
- [15] Aoki M, Kanemura S, Tsumura K and Yagyu K 2009 Phys. Rev.D **80** 015017 (arXiv:0902.4665 [hep-ph])
- [16] Grossman Y 1994 Nucl. Phys. B **426** 355 (arXiv:hep-ph/9401311)
- [17] Liu J and Wolfenstein L 1987 Nucl. Phys. B **289** 1
- [18] J. Hernandez-Sanchez, L. Lopez-Lozano, R. Noriega-Papaqui and A. Rosado, arXiv:1106.5035 [hep-ph].
- [19] See for instance: Dobrescu B 2001 Phys. Rev.**D63** 015004. See also, recent work on Little Higgs models: Arkani-Hamed N, Cohen A G, Katz E and Nelson A E 2002 JHEP **0207** 034. And for AdS/CFT Higgs models: Contino R, Nomura Y and Pomarol A 2003 Nucl. Phys. B **671** 148 (arXiv:hep-ph/0306259); Aranda A, Diaz-Cruz J L, Hernandez-Sanchez J and Noriega-Papaqui R 2007 Phys. Lett. B **658** 57 (arXiv:0708.3821 [hep-ph])
- [20] Kanemura S, Moretti S, Mukai Y, Santos R and Yagyu K 2009 (arXiv:0901.0204 [hep-ph])
- [21] Babu K S and Kolda C F 1999 Phys. Lett. **B451** 77 (arXiv:hep-ph/9811308)
- [22] S. L. Glashow and S. Weinberg, Phys. Rev. D **15**, 1958 (1977).
- [23] K. S. Babu and C. Kolda, Phys. Rev. Lett. **89**, 241802 (2002) [arXiv:hep-ph/0206310]; A. Dedes, J. R. Ellis and M. Raidal, Phys. Lett. **B549**, 159 (2002) [arXiv:hep-ph/0209207].
- [24] J. L. Diaz-Cruz and J. J. Toscano, Phys. Rev. D **62**, 116005 (2000) [arXiv:hep-ph/9910233]; J. L. Diaz-Cruz, JHEP **0305**, 036 (2003) [arXiv:hep-ph/0207030].
- [25] Kanemura S, Ota T and Tsumura K 2006 Phys. Rev. **D73** 016006 (arXiv:hep-ph/0505191); Kanemura S, Matsuda K, Ota T, Shindou T, Takasugi E and Tsumura K 2004 Phys. Lett. **B 599** 83 (arXiv:hep-ph/0406316)
- [26] C. D. Frogatt and H. B. Nielsen, Nucl. Phys. B **147**, 277 (1979).
- [27] H. Fritzsch, Phys. Lett. B **70** (1977) 436.
- [28] Diaz-Cruz J L, Noriega-Papaqui R and Rosado A 2005 Phys. Rev. **D71** 015014 (arXiv:hep-ph/0410391)
- [29] M. Gomez-Bock, R. Noriega-Papaqui, J. Phys. G **G32**, 761-776 (2006). [hep-ph/0509353].
- [30] Diaz-Cruz J L, Hernandez-Sanchez J, Moretti S, Noriega-Papaqui R and Rosado A 2009 Phys. Rev. **D79** 095025 (arXiv:0902.4490 [hep-ph]);
- [31] Fritzsch H and Xing Z Z 2003 Phys. Lett. **B 555** 63 (arXiv:hep-ph/0212195)
- [32] Cheng T P and Sher M 1987 Phys. Rev. **D35** 3484
- [33] Diaz-Cruz J L, Noriega-Papaqui R and Rosado A 2004 Phys. Rev. **D 69** 095002 (arXiv:hep-ph/0401194)
- [34] J. E. Barradas Guevara, F. C. Cazarez Bush, A. Cordero Cid, O. F. Felix Beltran, J. Hernandez Sanchez and R. Noriega Papaqui, J. Phys. G **37**, 115008 (2010) [arXiv:1002.2626 [hep-ph]]; A. Cordero-Cid, O. Felix-Beltran, J. Hernandez-Sanchez and R. Noriega-Papaqui, PoS **CHARGED 2010**, 042 (2010) [arXiv:1105.4951 [hep-ph]].
- [35] F. Cornet and W. Hollik, Phys. Lett. **B669**, 58 (2008).
- [36] E. Asakawa, D. Harada, S. Kanemura, Y. Okada, and K. Tsumura, Phys. Lett. **B672**, 354 (2009).
- [37] A. Arhrib, R. Benbrik, C-H. Chen, and R. Santos, Phys. Rev. **D80**, 015010 (2009).
- [38] K. Cheung and O. C. W. Kong, Phys. Rev. **D68**, 053003 (2003); H. N. Brown *et al.*, Phys. Rev. Lett. **86**, 2227 (2001); G. W. Bennet *et al.*, *ibid.* **89**, 101804 (2002); **89**, 129903(E) (2002).
- [39] G. V. Jikia, Nucl. Phys. **B412**, 57 (1994).
- [40] Shou Hua Zhu, Chong Sheng Li, Chong Shou Gao, Phys. Rev. **D58**, 015006-1 (1998); Zhou Ya-Jin, Ma Wen-Gan, Hou Hong-Sheng, Zhang Ren-You, Zhou Pei-Jun, Sun Yan-Bin, Phys. Rev. **D68**, 093004 (2003).
- [41] Sun La-Zhen and Liu Yao-Yang, Phys. Rev. **D54**, 3563 (1996); Shou-Hua Zho, J. Phys. **G24**, 1703 (1998).
- [42] G. t'Hooft and M. J. G. Veltman, Nucl. Phys. **B50**, 318 (1972); K. Fujikawa, B. W. Lee, A. I. Sanda, Phys. Rev. **D6**, 2923 (1972); B. W. Lee and J. Zinn-Justin, Phys. Rev. **D5**, 3121, 3137, 3155 (1972); **D7**, 1049 (1972).
- [43] K. Fujikawa, Phys. Rev. D **7**, 393 (1973).
- [44] C. G. Honorato and J. J. Toscano, Pramana **73**, 1023 (2009) [arXiv:0906.5139 [hep-th]].
- [45] M. Bace and N. D. Hari Dass, Ann. Phys. (NY) **94**, 349 (1975); M. B. Gavela, G. Girardi, C. Malleville, P. Sorba, Nucl. Phys. **B193**, 257 (1981); N. M. Moyonko, J. H. Reid, A. Sen, Phys. Lett. **B136**, 265 (1984); N. M. Moyonko and J. H. Reid, Phys. Rev. **D32**, 962 (1985); J. M. Hernández, M. A. Pérez, G. Tavares-Velasco, J. J. Toscano, Phys. Rev. **D60**, 013004 (1999); M. Baillargen and F. Boudjema, Phys. Lett. **B317**, 371 (1993); U. Cotti, J. L. Díaz-Cruz, J. J. Toscano,

- Phys. Lett. **B404**, 308 (1997). See also Ref.[9].
- [46] J. G. Méndez and J. J. Toscano, Rev. Mex. de Fís. **50**, 346 (2004).
 - [47] See for instance, U. Cotti, J. L. Díaz-Cruz, J. J. Toscano, Phys. Rev. **D62**, 035009 (2000); J. Hernández-Sánchez, M. A. Pérez, G. Tavares-Velasco, J. J. Toscano, Phys. Rev. **D69**, 095008 (2004).
 - [48] G. Tavares-Velasco and J. J. Toscano, Phys. Rev. **D65**, 013005 (2001). For a $SU_L(2) \times U_Y(1)$ -covariant formulation of a nonlinear gauge-fixing procedure for the new gauge bosons predicted by 331 models, see J. Montaña, F. Ramírez-Zavaleta, G. Tavares-Velasco, and J. J. Toscano, Phys. Rev. **D72**, 055023 (2005); F. Ramírez-Zavaleta, G. Tavares-Velasco, and J. J. Toscano, Phys. Rev. **D75**, 075008 (2007).
 - [49] J. L. Díaz-Cruz, J. Hernández-Sánchez, J. J. Toscano, Phys. Lett. **B512**, 339 (2001).
 - [50] J. F. Guion and H. E. Haber, Phys. Rev. **D67**, 075019 (2003).
 - [51] S. Kanemura and H. -A. Tohyama, Phys. Rev. **D57**, 2949 (1998); S. Kanemura, Phys. Rev. **D61**, 09501 (2000); Eur. Phys. J. **C17**, 473 (2000).
 - [52] Borzumati F and Greub C 1999 Phys. Rev.D **59** 057501 (arXiv:hep-ph/9809438)
 - [53] Xiao Z J and Guo L 2004 Phys. Rev.D **69** 014002 (arXiv:hep-ph/0309103)
 - [54] Bowser-Chao D, Cheung K M and Keung W Y 1999 Phys. Rev.D **59** 115006 (arXiv:hep-ph/9811235)
 - [55] Wahab El Kaffas A, Osland P and OGREID O M 2007 Phys. Rev.D **76** 095001 (arXiv:0706.2997 [hep-ph])
 - [56] Isidori G 2007 (arXiv:0710.5377 [hep-ph])
 - [57] Diaz-Cruz J L *et al.* in preparation
 - [58] Mahmoudi F and Stal O 2009 (arXiv:0907.1791 [hep-ph])
 - [59] Chankowski P H Krawczyk M and Zochowski J 1999 Eur. Phys. J. C **11** 661 (arXiv:hep-ph/9905436)
 - [60] Haber H E and Logan H E 2000 Phys. Rev. D **62** 015011 (arXiv:hep-ph/9909335); Logan H E (arXiv:hep-ph/9906332)
 - [61] K. Nakamura *et al.* [Particle Data Group], J. Phys. G **37**, 075021 (2010).
 - [62] J. -M. Gerard and M. Herquet, Phys. Rev. Lett. **98**, 251802 (2007) [hep-ph/0703051 [HEP-PH]]. S. de Visscher, J. -M. Gerard, M. Herquet, V. Lemaitre and F. Maltoni, JHEP **0908**, 042 (2009) [arXiv:0904.0705 [hep-ph]].
 - [63] Abulencia A *et al.* [CDF Collaboration] 2006 Phys. Rev. Lett. **96** 042003 (arXiv:hep-ex/0510065)
 - [64] For a review see: Borzumati F and Djouadi A 2002 Phys. Lett. B **549** 170; Roy D P 2004 Mod. Phys. Lett. A **19** 1813
 - [65] Kanemura S, Kubota T and Takasugi E 1993 Phys. Lett. B **313** 155 (arXiv:hep-ph/9303263); Horejsi J and Kladravá M 2006 Eur. Phys. J. C **46** 81 (arXiv:hep-ph/0510154); Akeroyd A G, Arhrib A and Naimi E M 2000 Phys. Lett. B **490** 119 (arXiv:hep-ph/0006035)
 - [66] R. Mertig, M. Böhm, A. Denner, Comput. Phys. Commun. **64**, 345 (1990).
 - [67] A. Barroso, F. Boudjema, J. Cole and N. Dombey, Z. Phys. C **28** (1985) 149.